Certificate

Certified that the contents and form of the thesis entitled

"Characterization of Pyroelectric Thin-Films and Nano-Fibres for Effective Energy Harvesting from Solar Cells"

Submitted by

Mr. Zain Ali

Has been found satisfactory for partial fulfilment of the requirements of the degree of Master of Science in Environmental Sciences.

Supervisor:.....

Dr. Muhammad Fahim Khokhar

Professor

IESE, SCEE, NUST

GEC Member:……

Dr. Nadia Shahzad

Assistant Professor

USPCAS, NUST

GEC Member:……

Dr. Yousuf Jamaal

Assistant Professor

IESE, SCEE, NUST

Thesis Acceptance Certificate

Certified that final copy of MS/MPhil Thesis written by **Mr. Zain Ali (Registration #00000172376)** of IESE (SCEE) has been vetted by undersigned, found complete in all respects as per NUST Statues/Regulations, is free of plagiarism, errors, and mistakes and is accepted as partial fulfilment for award of MS/MPhil degree. It is further certified that necessary amendments as pointed out by GEC members of the scholar have also been incorporated in the said thesis.

Supervisor & (Head of Department): _____

Prof. Dr. Muhammad Fahim Khokhar

Dated: _____

Principal: _____

Dated: _____

Declaration

I certify that this research work titled *"Characterization of Pyroelectric Thin-films and Nano-fibres for effective energy harvesting from Solar Cells"* is my own work. The work has not been presented elsewhere for assessment. The material that has been used from other sources, has been properly acknowledged/ referred.

……..

Zain Ali

00000172376

Plagiarism Certificate (Turnitin Report)

This thesis has been checked for Plagiarism. Turnitin report endorsed by supervisor is attached.

Signature of Student

Zain Ali

00000172376

……..

Signature of Supervisor

Acknowledgements

In the name of Allah, the Most Gracious and the Most Merciful, all praises to Him for the strengths and blessing in completing this thesis.

I would like to express my gratitude to my supervisor, ***Dr. Muhammad Faheem Khokar***, for his consistent support, patience guidance, appreciation and motivation throughout my research work. I have been extremely lucky to have a supervisor who cared so much about my work, and who responded to my questions and queries so promptly.

I would also like to thank and express my gratitude to ***Dr. Nadia Shahzad*** *and* ***Dr. Yousuf Jamal*** for their help, encouragement and insightful comments. In particular I would also like to acknowledge lab engineer ***Mr. Amir Satti*** *and* ***Muhammad Asghar*** *and* ***Dr. Sehar Shakir*** *(AEMS LAB USPCASEN)* and seniors of this institute to whom I am indebted for their help. My special thanks to ***Noor Haleem*** lab demonstrator *(Advance Analytical Lab IESE)* for assisting me time to time whenever I needed their guidance and help.

And at the last but not the least, I would like to express my gratitude to my parents, siblings beloved fiancée and friends ***Ramiz Izhar***, ***Zubair Jameel***, ***Jahanzaib Ahmad, Noman Bhatti, Muhammad Hanif,*** and ***Humayoon Jallat*** for believing in me and being there for practical support whenever I needed it and for helping me to keep things in perspective.

Zain Ali

Dedication

This thesis is dedicated to my loving and supportive ***Mother*** *whose tremendous encouragement and cooperation led me to this delightful accomplishment.*

Abstract

Energy harvesting from solar-cell with high efficiency has great attention from the last few decades. For this purpose, the addition of pyroelectric materials which have the ability of polarization with the change in temperature used as an interlayer between absorber and anti-reflection layer. Pyroelectric polymers can effectively improve the photovoltaic performance of solar cells. It can induce an electric field to promote the dissociation of electron-hole pairs, and the generated charge is collected from the opening. This enhancement in performance requires that the material have a unique crystal structure to polarize it at low energy. Multiple approaches are used to collect higher β-phase content, we herein assess a route to crystalline polyvinylidene fluoride (PVDF) electrospun nanofibers and thin-films based on electrospinning and spin coating method. The significant feature of the above method is that PVDF and blende of carbon black and PVDF are mixed into an acetone/DMF solution, and a thin film with high thermoelectric β phase content is prepared by Spin-coating and Electrospun. However, the characterization of electrospun nanofibers with FTIR and XRD shows that the crystallinity is significantly higher i.e. β-phase content. We find that the nanofibers prepared by electrospinning have more electroactive β-phase content than spin-coated films. Therefore, the organic pyroelectric nanofibers and thin films with controlled boundaries proposed in this study are very suitable for a wide scope of optoelectronic applications.

Key Word

Electromagnetic Radiation

Pyroelectric

Ferroelectric

Polyvinylidene fluoride (PVDF)

Solar Cells

Photovoltaics (PV)

Billion Standard Cubic Feet (BCF)

Deposition Techniques

Thin-films

Nanofibers

Electrospinning (ES)

Spin-coated (SC)

Fourier transform Infrared Spectroscopy (FTIR)

X-ray Diffraction (XRD)

Scanning Electrons Microscopy (SEM)

UV-Visible Spectroscopy

Hall-Effect

Resistance

Conductivity

Mobility

Figure of Merits (FOM)

Solar cell efficiencies

Conference of Parties (COP)

Greenhouse Gases (GHG)

List of Figures:

List of Tables

Table of Equations

Table of Contents

Chapter 1

INTRODUCTION

1.1. Background:

According to a research by the World Energy Council, due to the swift progress of the world economic development after the Industrial Revolution and the population growth in countries for instance United States, China, India, and Pakistan, 18 terawatts (TW) of energy were used globally in 2018 According to a survey of world energy council 18 TW energy was used globally in 2018, due to rapid growth in the world economy and population in countries such as China, India and Pakistan. With the existing energy policies, worldwide energy demand increases by 45% until 2035 (Lare, 2014). Pakistan is also facing a massive energy crisis, which lacks in natural gas about two billion standard cubic feet (BCF) and 3,000-6,000 megawatts (MW) per day. Therefore, the energy model becomes unstable in meeting the gap between supply and demand (Lare, 2014).

While the combustion of hydrocarbon fuels also increases the concentration of carbon dioxide, methane and other greenhouse gases, leading to global warming and air pollution (Yan et al., 2019). After the COP-21 World global energy trends have shifted to renewable energy sources that respond to climate change. Therefore, other than the existing energy models which are based on fossil fuels, we also need state-of-the-art equipment with higher efficiency. In the past few decades, renewable energy has attracted much attention (Yan et al., 2019).

There are still many shortcomings in finding new sources of fossil fuels and producing useful products from them, which requires a lot of effort and capital. Therefore, this is a laborious, time-consuming and risky effort. Because of many external factors, such as environmental problems and economic feasibility. Coal shovel, onshore drilling of oil, and offshore drilling of oil are often complete wastage of resources such as KEKRA-1 offshore drilling of oil in the deep sea of Karachi caused a loss of 14 billion PKR (Siddiqui, 2019).

1.2. Problem statement:

Now it has become critical to cut the consumption of fossil energy and add new alternative green energy sources in national grid, which is highly appreciated (Yan et al., 2019). About 33% of the world ’s renewable energy is being produced, and future productivity is expected to increase (Khursheed et al., 2019). The main contributors are Solar photovoltaics (PVs) to these renewable energy sources (Khursheed et al., 2019). But the main problem of photovoltaic cells is their efficiency in terms of manufacturing cost and

energy conversion from solar electromagnetic radiation to useable energy. There are various existing technologies for converting solar energy into usable thermal energy in solar photovoltaic systems, portable systems, wearable electronic products, and solar rechargeable batteries. But to improve their efficiencies more research and development is required. This research is also an effort for progress in the efficiency for solar panels by introducing pyroelectric films and nano-fibers above the absorber layer.

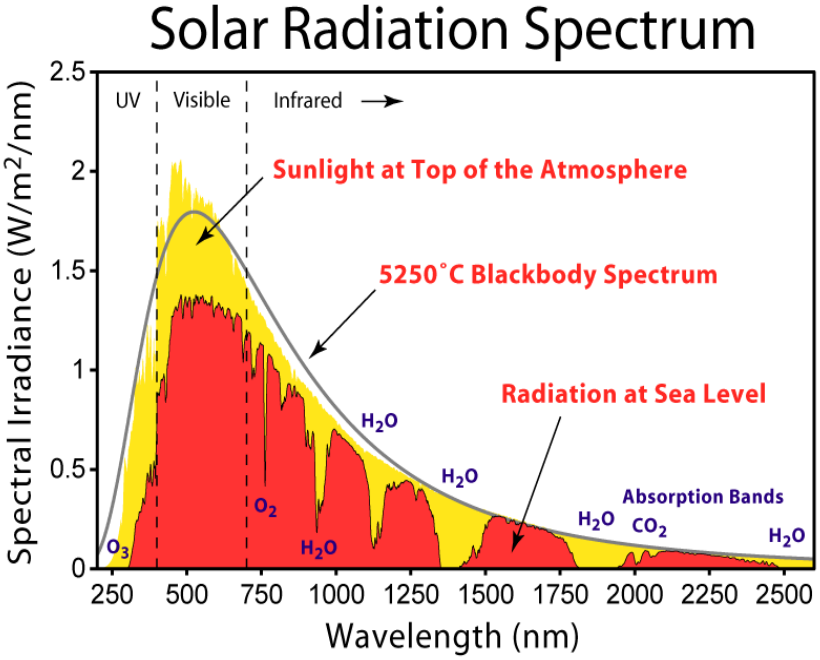

Figure 1.1: Solar irradiance spectrum above the atmosphere and at the surface (Ranabhat et al., 2016)

The main idea behind this additional layer of pyroelectric material to convert thermal fluctuations into electrical energy. Study of materials with pyroelectric properties includes, the research of their thermodynamic properties of a crystals, In which a series of dense and comprehensive crystal state variables, namely electrical, thermal, magnetic and mechanical field (Jachalke et al., 2017).

The pyroelectric effect describes the change in temperature "T" which can impose a spontaneous polarization "P_S" related to certain crystalline substances (Jachalke et al., 2017). There are different materials which exhibit this characteristic. Such materials are being employed in waste heat harvesters temperature and motion detectors, electrocaloric cooling, pyro-electrocatalytic disinfection, X-ray generator, radical and hydrogen production, as well as infrared radiation.

The reason is their pyroelectric behaviour, which is why we can add such materials to solar cells, and when solar radiation cannot be directly available for solar cells, we can collect

energy from minimal temperature changes. Furthermore, we can use such a PV system in the area where solar irradiance is a very minimal or colder region.

In this study: we used polyvinylidene fluoride (PVDF) ferroelectric polymer, which have excellent piezoelectric, pyroelectric and ferroelectric nature. PVDF is in between various crystal phases, namely α, β, γ and δ. The maximum value of crystalline phase is β-type PVDF, and the crisscross (all trans) shape (TTT) indicates the maximum polarity (Zhang et al., 2017a). Due to these change in molecular shape, this is why PVDF has unique ferroelectric properties.

1.3. Energy needs and Climate Change:

Global energy trends are based on fossil fuels, leading to global warming and climate change. To overcome this problem, we must reduce greenhouse gas emissions and change our source from non-renewable to renewable with more eco-friendly greener technologies. For this purpose, a conference was held in Paris in 2015. At this summit, massive energy consumers such as China, the United States and India and 194 countries signed the first global agreement on climate change in history. These negotiators committed to outlining the long-term development strategy of lower greenhouse gas emissions. The climate agreement has its "Agenda for Action" to ensure more significant progress in achieving accelerators beyond binding commitments (GFSE, 2016).

The purpose is to control the average global temperature to a level below 2°C and above the pre-industrial level to ensure that the temperature is limited to 1.5°C. In order to achieve the above goals, all countries are required to review their contribution to reducing greenhouse gas emissions in the Paris Agreement every five years. Every new contribution made at the national level should strictly cover progress compared to precedent. Both sides agreed to reach the highest global level of greenhouse gas emissions in order to strike a balance between emissions and removals. Countries also demand accelerated efforts to reduce and reduce greenhouse gas emissions (GFSE, 2016).

Before delving into the details, we need to understand what factors distinguish renewable energy from non-renewable energy, how do they relate to population and economic growth, and how do they affect our environment? Non-renewable energy depends on the burning of fossil fuels, which leads to the emission of greenhouse gases (GHG), productivity and energy consumption both are the hot topics in climate change (Bölük & Mert, 2014). According to the current figures from the EU-JRC (Joint Research Center), the utilization of fossils accounts for 90 percent of global carbon dioxide emissions, and the results are

surprising. The correlation between economic growth, demand of energy and ecological pollution has been studied in past few years. (Bölük & Mert, 2014).

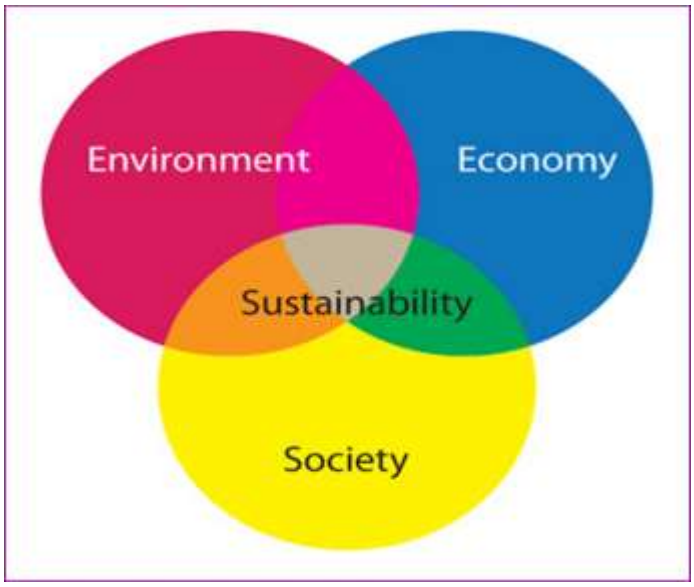

Figure 1.2: Sustainability Ven Diagram (Circularecology)

On the different side, several renewable and eco-friendly energy resources like wind turbines, hydroelectric power plants and photovoltaic systems will not cause any greenhouse gas emissions. According to (Bölük et al., 2014), the green energy sources are the rapidly emergent sources in all over the globe, and it is expected to increase from 10% in 2008 to 14% of the total energy sources in 2035. Various countries around the world focus on renewable energy due to fluctuations in oil prices, dependence on exported energy with energy security issues, and the effect of greenhouse gases on the environment have become a worrying issue. To ensure sufficient investment in the field of renewable energy, various incentive mechanisms are taken into account to support the renewable energy market (Bölük & Mert, 2014). More than 100 countries have set their own goals and formulated key policies on renewable energy (Bölük et al., 2014). For renewable energy in global development techniques based on market and non-market promotion have been introduced. It included tariff rates, bonuses, share-based green certificates, tender incentives, investment incentives, tax exclusions and concessions and various government places. The global response to government renewable energy support increased from the US $ 41 billion in 2007 to the US $ 88 billion in 2011 (Bölük et al., 2014).

1.4. Solar Energy Systems:

The sun is the main energy source in our solar system, providing energy to the earth in the form of electromagnetic radiation. These solar radiations support life and can be converted into usable energy more efficiently through reliable selection. It is an easy-going and

environmentally friendly energy source with great potential for conversion into useful energy(Summary, 2016).

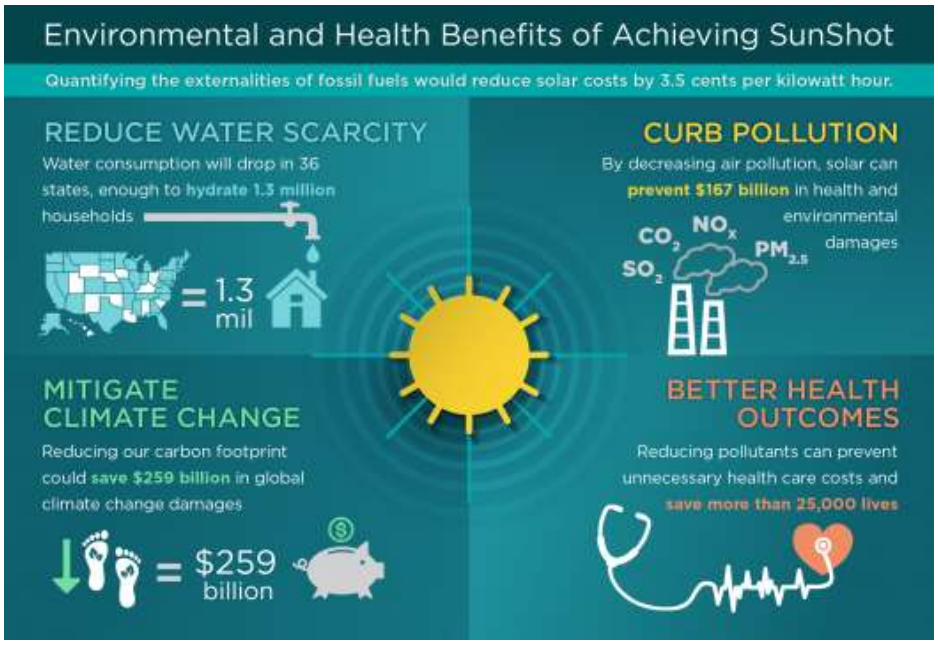

Figure 1.3: "On the Path to SunShot report series". (office of energy efficiency & renewable energy)

The report on the environmental and public health benefits of the high popularity of solar energy in the United States highlights how increasing the amount of solar energy connected to the grid will affect the environment by reducing water shortages, curbing pollution, mitigating climate change and creating better health conditions advantageous result. This is why solar energy systems are now one of the main sources of energy harvesting. In order to develop new solar energy collection equipment, such as "photovoltaic systems", understanding of the basic properties of semiconductors and conventional solar cells. Bell Labs manufactured the first batch of crystalline silicon solar cells in 1953, with an efficiency of 4.5%, and subsequently manufactured devices with an efficiency of 6% in 1954 (Saga, 2010). Comparing conventional solar cells with new solar cells can help increase efficiency, reduce manufacturing costs and energy consumption to manufacture industrial solar cells (Soga, 2006).

Despite the rapid decline in photovoltaic costs, there are still many gaps in the development of more efficient, low-cost, ultra-light, and malleable materials, which can reduce photovoltaic installation costs (Summary, 2016).

In terrestrial environments, bulk monocrystalline or polycrystalline silicon solar cells are used. The structure of a typical solar cell consist on about 300 μm thick p-type substrate and less than 1 μm thin n-type emitter layer (Soga, 2010). Nanomaterials can increase

incident radiation by a factor of nine times and the productivity of solar collectors will be ten times higher than traditional solar panels (Abdin et al., 2013).

1.5. Energy Conversion Principle in Solar Cell:

The working of solar cells is linked with the basic principle of photovoltaic effect. When incident solar radiation strikes a semiconductor material (with certain internal structure and characteristics), it will generate electrical energy. The effect is related to the photoelectric effect, in which the light-absorbing material emits electrons at a higher frequency than the threshold frequency associated with the material and generates electron-hole pairs. Albert Einstein was the man who explained the photoelectric effect in 1905, thinking that light is composed of energy packets or quanta commonly known as photons. Their energy can be computed as:

$$E = h\upsilon \quad \text{Equation 0.1}$$

The frequency of light is "υ" and Planck's constant is represented by "h". This interpretation of the photovoltaic effect was a breakthrough in physics. In solar cells, the energy conversion of light (i.e. ultraviolet, visible, and infrared) requires some steps to generate voltage. Absorber layers of the material absorb light which causes a change of state of materials from the ground to an excited state, Direct current is:

1. Emitted electrons cause formation of positively charged vacancies or holes and free negatively charged carriers in the material
2. Channelization mechanism of positive charges toward the anode while the contact direction of the free negative charge carrier is toward the cathode
3. At this stage, high-energy free negative charge carriers reach the cathode, causing electrons to lose energy following an external path and complete useful electrical load work, then return to the anode and complete the final step of the cycle
4. Combine with the free positive charge carriers of the absorber to return to the ground state (Fonash, 2010)
5. Most solar radiation is absorbed or reflected by solar cells. Absorbed solar radiation will increase the temperature, increase the opposite saturation current, decrease the open circuit voltage, and reduce the energy gap. (Abdin et al., 2013).

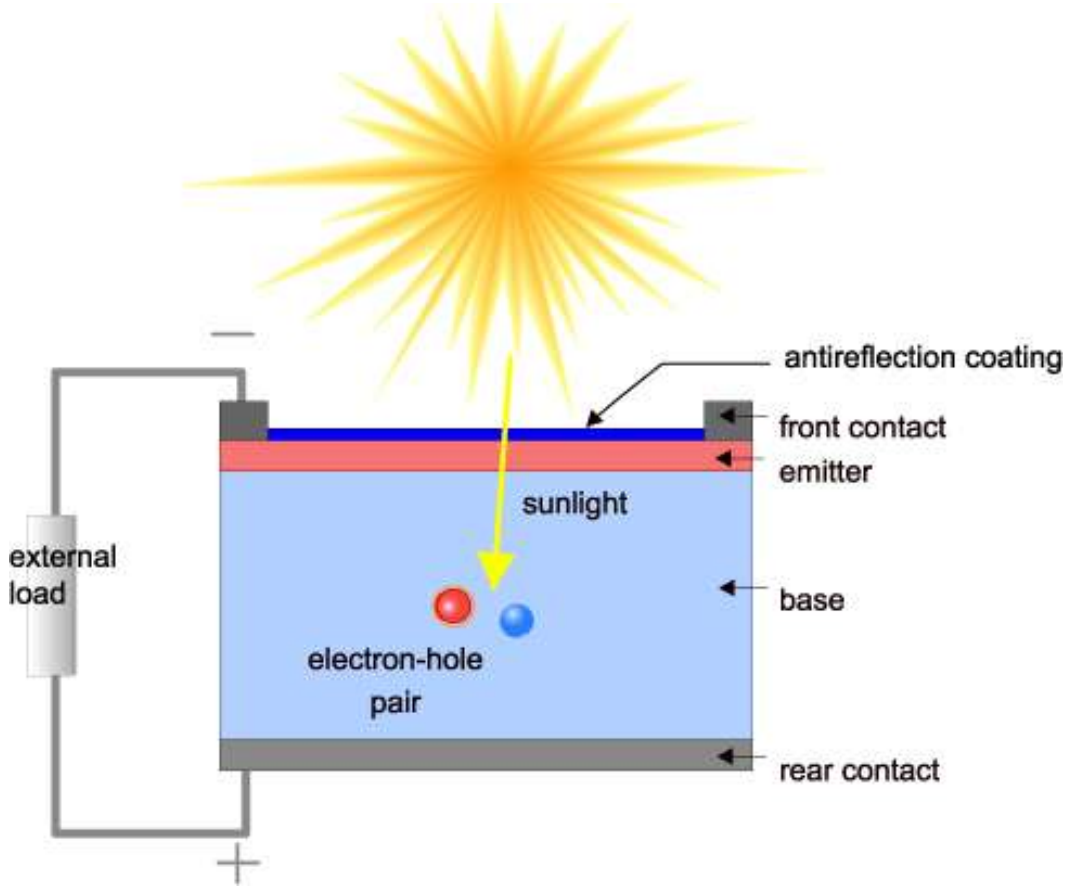

Figure 1.4: Cross sectional view of a solar cell (pveducation)

Inability of conversion photons below the band gap to electrical energy, and the inability to heat the photon energy beyond the band gap are the dominant loss mechanisms in a single band gap solar cell. These two mechanisms create half of the solar energy loss during conversion. Therefore, the thermodynamic limit is the point of consideration to get maximum efficiency of single junction solar cell. Shockley and Queisser calculated the single band gap limit in 1961.

1.6.Types of Solar Cells Technologies:

Depending on the manufacturing method, final shape of solar cells and materials use for semiconductors there are different types of solar cells (Prashant, 2018). For example, monocrystalline polycrystalline amorphous and tandem panels. Because of advanced fabrication technologies of solar cell, like dye-sensitized solar cells (DSSC) and other Novel types of solar cells have also made many advances.

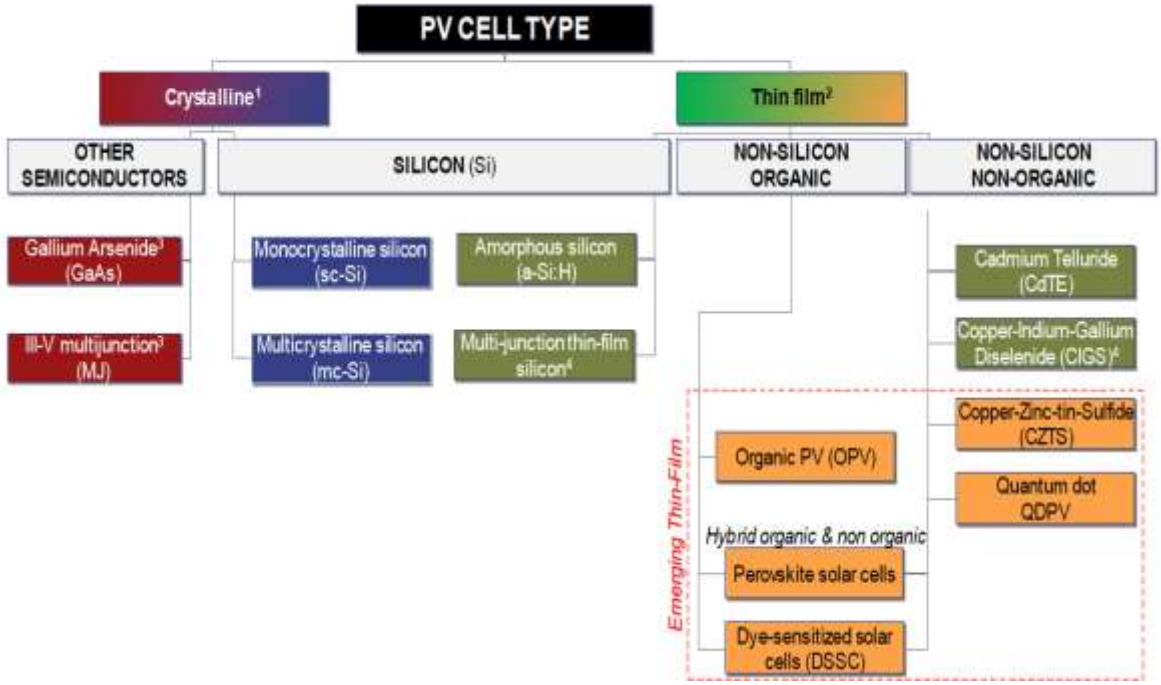

Figure 1.5: Types of solar cells. "(IPCC, 2011," special report on renewable energy (MIT, 2015)

1.6.1. Crystalline Solar Cells:

These type of photovoltaic cells are most demanding solar cells in the market, because of their higher conversion efficiency as compared to other commercially available solar cells (Saga, 2010).

1.6.1.1. Mono-Crystalline Panels:

Monolithically crystallized silicon bars are units of these panels. Their efficiency does not reach more than 24.7% in ideal scenarios and 23% in commercial use (Prashant, 2018).

1.6.1.2. Polycrystalline Panels:

Polycrystalline silicon resembles with the earlier type (monocrystalline silicon), but crystallization process is different in these types of solar cells. Disordered crystals of silicon based design employees in the polycrystalline panels. They have lower efficiency than monocrystalline, laboratory and commercial modules have about 19.8% and 14% of power conversion efficiency respectively (Prashant, 2018). The price of these panels are relatively low.

1.6.1.3. Amorphous Panels:

Amorphous silicon units dominate under warm and unclouded environments because their temperature coefficient for power loss is very low. In case of amorphous solar panels: utilizing silicon with other semiconductor material which give different type of structure. These panels have an extensive thickness so more slim and flexible panels can be

fabricated. Sometimes, these panels can be habituated to irregular surfaces. They are known as amorphous photovoltaic solar panels or sometimes we call them thin-film photovoltaic modules. The classification of these thin-film solar cells is according to the materials used.

1.6.1.4. Amorphous Silicon (TFS):

They are also made of silicon: nevertheless, unlike the prior examples in this case the material does not have a crystalline arrangement. These panels are generally used in small electronic products (baby toys, calculators, watches) and small portable arrays. Their highest performance in the laboratory and commercial modules is about 13%, and 8% respectively. Commercial component performance for Cadmium-telluride in the laboratory is 16% and 8%. In commercial panels one of the most effective materials is Gallium arsenide with an efficiency of 20%.

1.7.Thin Film Solar Cells:

1.7.1. Tandem Panels:

There are some other types of panels which are in series arrangement and formed by doping two discrete types of semiconductor materials. Every material is specific in wavelength i.e. only a small window of solar radiation will absorb by them, consequently, if we use blend of two or three types of materials which can be used to collect different electromagnetic spectrum. Efficiency of such panels can be as high as 35%.

1.8.Types of materials used for PV systems:

Solar cells use the solar spectrum and convert sunlight into electrical energy. Different materials such as silicon, cadmium sulfide and organics are used to utilize the largest part of the spectrum. Materials are categories in different classes and sub-classes i.e. Dielectric and its subclasses are Piezo, Pyro, Ferroelectric all of the different ways to convert different type of energies into electrical energies. It depends on the crystal lattice (Bhavanasi, et al., 2014).

Polyvinylidene fluoride (PVDF) and their co-polymers are organic ferroelectric materials. Which commonly used in the manufacture of microfiltration devices, ferroelectric field effect transistors, non-volatile memories, battery separators, piezoelectric energy harvesters etc. (Barber et al., 2009). Polymer of PVDF has a chemical formula $-CH_2-CF_2-$ and at least five phases called α, β, γ, δ. and ε The structure and nature of these stages are well documented in the literature (Costa, et at., 2010). It was found that PVDF nanofibers are more suitable for fabrication of piezoelectric energy harvesting devices than thin films (Barber et al., 2009).

1.9. Pyroelectric Effect:

There is a diverse range of Pyroelectric materials from a crystals to ceramics and polymers to thin films, and have inorganic or organic properties (Jachalke et al., 2017). Many figure of merit (FOM) was introduced for characterization of the of pyroelectric materials. These different materials have the pyroelectric coefficient value of "p", which describes the ratio between the change in polarization P_S with respect to time "T". Consequently, the exact derivation of the value of *"p"* is a key part in equipment formation and upgrading. Temperature dependent $\boldsymbol{p_{(T)}}$ discloses additional facts, for example the phase change temperature, which restrict the temperature array of the device. In addition, temperature dependent value of *"p"* is significant for material growth, e.g. to study the impact of blending or arrangement changes (Jachalke et al., 2017).

1.9.1. Mathematical description:

The pyroelectric coefficient is described under specific conditions suchlike constant electric field , stress and change in the spontaneous polarization vector with temperature:

$$\boldsymbol{\rho = (\partial D/\partial T)_{\sigma,E} = (\partial P/\partial T)_{\sigma,E}} \quad \textbf{.....Equation 0.2}$$

Where D is the dielectric displacement, *P* is the polarization, and σ and E represent continuous pressure and continuous electric field, respectively. Physically speaking, the internal structure of the electric dipole in the thermoelectric material will change during temperature changes, such as the rotation or reorientation of the molecular dipole or the atomic arrangement of the replacement ferroelectric crystal. This leads to a change in spontaneous polarization and a subsequent transformation in the charge on the surface of the material.

1.10. Importance of β-phase in PVDF:

PVDF have different crystal shapes i.e. α, β, γ, δ and ε phases according to unlike procedures (Ruan et al., 2018). Because of the antiparallel stacking of dipoles, the α and ε phases are non-polar (Ruan et al., 2018). While remaining three PVDF crystals are polar and shows pyroelectric and ferroelectric properties (Cai et al., 2017). The properties and wide application of α, β and γ phase PVDF were studied. The easy availability of α-phase PVDF has aroused wide interest in the research of PVDF melt crystallization and α to β phase transition(Cai et al., 2017). The PVDF has different polymorphs: according to the molecular chain conformation in the manufacturing process, α (TGTG', Form II), β (TTTT, Form I), γ (T_3GT_3G', Form III), while nonlinear structure depend on processing in δ and ε phase (Cai et al., 2017).

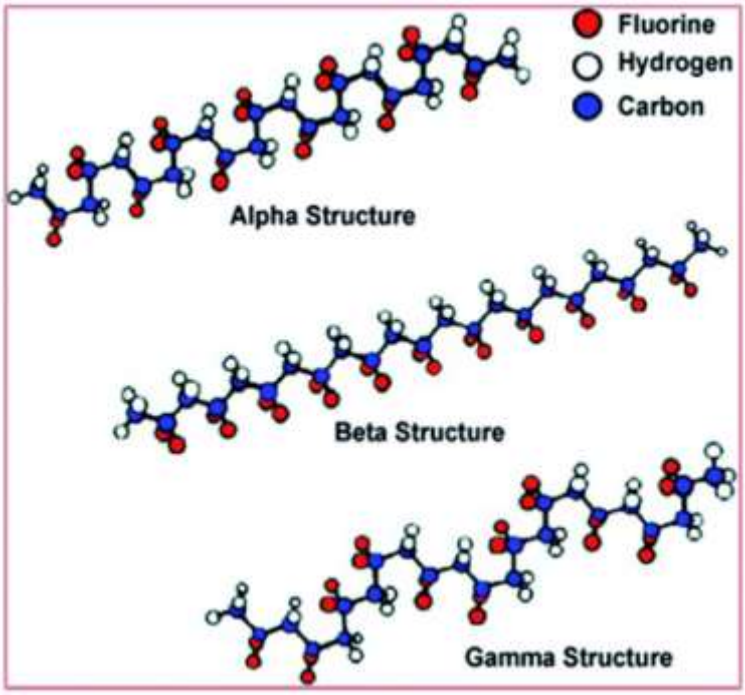

Figure 1.6: Structure of α, β & γ phases (Ruan et al., 2018)

So, we need more β-phase in our thin-films and electrospun fibers for its high electroactive and optical properties. The formation of α and β phases is mainly related to the evaporation rate of the solvent. High rate is conducive to the formation of α phase, while low rate is conducive in the creation of β phase (Costa et al., 2010).

1.11. Research Objectives:

The objective of this thesis is the following:

1. To synthesize and deposit the thin-films and nano-fibers of PVDF on the substrate
2. To get more crystalline phase i.e. β-phase in PVDF
3. To characterize the thin film by different techniques
4. To analyze the effectiveness of the developed pyroelectric films for application in solar cells

Chapter 2

LITERATURE REVIEW

Due to global energy demand (S. B. Kang et al., 2017) and the effect of burning of fossil fuels renewable energy sources have been great attention (K. Choudhary et al., 2019). Organic photovoltaics (OPVs) or organic solar cells (OSCs), a subset of these energy sources, is made of the thin film of organic semiconductor materials and have received exceptional attention as a substitute to their inorganic equivalents for the generation of affordable and clean renewable energy(Petrus, 2009). In the recent scenario, power conversion efficiencies have been achieved up to 17% for both single- and tandem-junction OSCs (Petrus, 2009).

2.1. Solar Cells Generations:

Solar cells are divided into three generations in an outstanding order. Three generations conduct research simultaneously to increase efficiency

2.1.1. First Generation:

High-quality large-area and single-junction structure are key attribute of first-generation solar cells (Conibeer, 2014). The first generation of technology involved a lot of energy and labor input, which hindered major progress in rapid declining of production costs. Single junction silicon panels are impending to theoretical limit of 33% efficiency, that is, 33% of sunlight falling on the solar cell is converted into electricity (Conibeer, 2014). The theoretical limit is calculated using device limitation in terms of wavelength, electron-hole pair generation, and recombination and diffusion lengths (Mozumder et al., 2019). Though the solar cells of this generation are accounted for the majority marketable production for approximately 89.7% in 2007 (Choubey et al., 2009).

2.1.2. Second Generation:

The materials used in second generation were created to address the energy needs and construction costs of cells (Abdin et al., 2013). Alternative manufacturing techniques (such as vapor deposition and electric coating) are advantageous because they can significantly reduce processes at high temperatures (Summary, 2016). It is generally believed that with the development of manufacturing technology, manufacturing costs will be determined by the supplies of the constituent materials (Sengupta et al., 2018). Under the circumstances familiar to III-V device manufacturers, the scope of the main cost reduction is limited by the cost of substrate (Conibeer, 2014). Mature thin-film method may replace first-generation technology (Conibeer, 2014).

The second generation takes the example of Pacific Solar's module using polycrystalline silicon on glass in the Sydney pilot production line (Conibeer, 2014). However, the efficiency limit of the second generation is 15%, far below the 93% limit (Conibeer, 2014). The material was developed to meet the energy needs and costs of solar cell production (P. Choudhary et al., 2019) these materials are commonly used in this thin film technology for example cadmium telluride, copper indium gallium arsenide, amorphous silicon and microporous silicon (Mozumder et al., 2019). Which reduce the quality and consequently cost by creating a substrate that chains glass and glass ceramics (Li, et al., 2020). They also achieve maximum energy conversion efficiency. The trend from the first generation to the second generation is emerging, but it turns out that the commercialization of the technology is difficult (Sengupta et al., 2018). Research and development on solar cell to improve efficiency by increasing output voltages and taking it closer to thermodynamic boundaries had led to the progress of third-generation cells (Conibeer., 2014). Advancement in deprived electrical properties of the film, this technology is used in conjunction with other technologies that enable low production costs and is a non-semiconductor technology (K. Choudhary et al., 2019).

2.1.3. Third Generation:

Non-semiconductor technologies in third-generation panels include non-semiconductor structures, for instance quantum dot, series/multi-junction, hot carrier cells, up-down conversion and conversion technologies (Choubey, et al., 2009). PV constructed from multiple cells is a current route (Landsberg et al., 2017), integrated series battery involving up to three different band gap batteries has been produced for the spacecraft, with an energy conversion efficiency of up to 30%(Conibeer, 2014). Low-size semiconductors also have great potential for increased flexibility (Terakawa, 2013). The current research goal is to maintain 30-60% conversion rate though retentive low-cost materials and manufacturing technologies (Mahesh et al., 2012). There are several ways to achieve these high efficiencies (Landsberg et al., 2017). The multi-junction method might effect in the concentrator efficiency exceeding 40%, thereby expanding the advantages of III-V PV and exceeding the 30% efficiency limit of silicon (Conibeer, 2014).

2.1.4. Solar Cell Research and Development:

The firm expansion of the photovoltaic engineering is due to the production mechanization of thin-film solar cells with better efficiency (P. Choudhary et al., 2019). The call for innovations in the photovoltaic manufacturing from time to time stop due to developments in manufacturing technologies, resulting in increased cost affordability and development

of the photovoltaic market (IRENA, 2019). By breaking old boundaries of efficiency and cost by attaining novelty using advance knowledge of physics and materials science will become a revolution (Schmidt et al., 2019). It has been shown that nanotechnology is the most powerful source of increasing solar efficiency, sustainable energy and storage by many years of study (Abdin et al., 2013). New dielectric materials that use nanotechnology have a wide range of applications for energy harvesting and loading systems (such as portable electronic instrument, hybrid electric automobiles (HEA), and throbbed power structures), so they are in great demand (Barber et al., 2009).

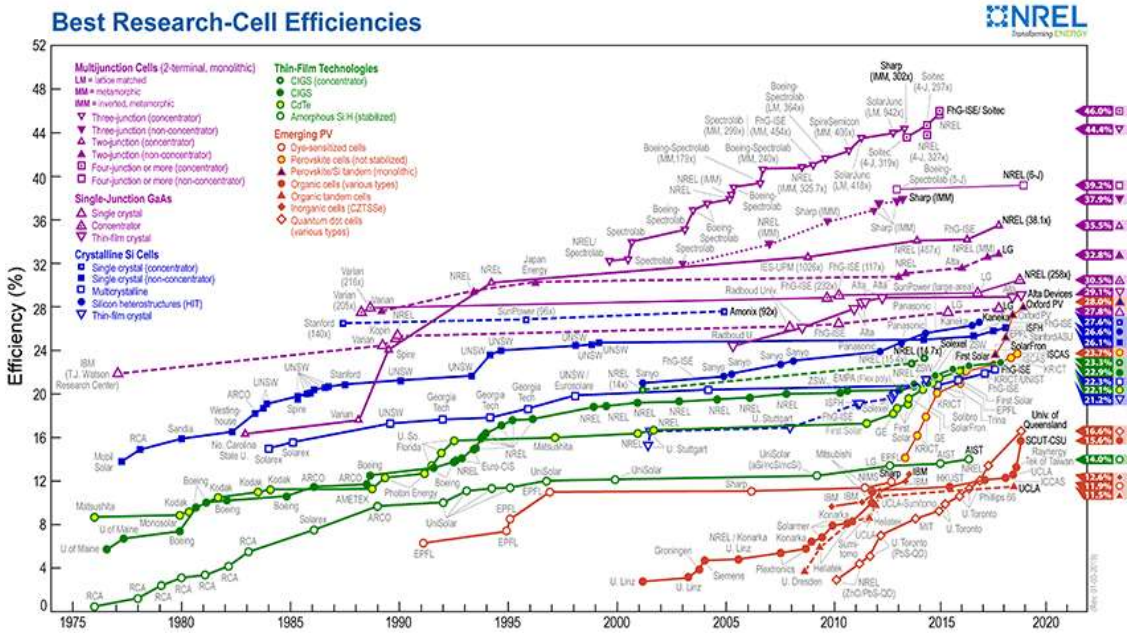

Figure 2.1 Solar cell efficiencies for various technologies under standard conditions (NREL)

Recently, there have been extensive attempts to progress in the conversion efficacy of solar cells by introducing pyrolysis and ferroelectric organic materials and their copolymers. (Sengupta et al., 2018). This method requires that: these organic ferroelectric substances have a unique unprotected film structure because a pair of photoelectron holes must be passed through the holes of the sequestering ferroelectric polymer (Matabola et al., 2013). Acquire extraordinary photovoltaic efficiency by addition of ferroelectric carbon-based materials between the anode of the solar cell and the dynamic coating of the bulk (S. B. Kang et al., 2017). As a result, the interface will be divided into ferroelectric regions (strong electric fields) and electrode regions (making photovoltaic charges flow) (Sharma et al., 2016). Therefore, controlling the coverage of the ferroelectric layer may be important for improving photovoltaic efficiency (Landsberg et al., 2017). Notwithstanding legitimate shape, ferroelectric polymer films utilized as solar cell interlayers can likewise display high crystallinity and ferroelectric phase materials. (Haider et al., 2018).

Organic thin films prepared by different organic deposition techniques e.g. Electrospinning, Langmuir–Blodgett (LB) and spin coating methods which can further use as organic solar cell interlayers electrospinning method will significantly enhance due to its excellent crystal latency and ferroelectric phase content, solar cells have high efficiency (Rex et al., 2019). In contrast, the spin-coating film has low crystallinity and ferroelectric content, so it cannot effectively improve battery efficiency because it will act as an insulator rather than a ferroelectric material (S. J. Kang et al., 2008). At the same time, the reduce PVDF has a high melting point, which makes it a potential melting point and can be used as a thermoelectric and ferroelectric material at high temperatures. (Zhang et al., 2017). Electro-spin fibers have shown a number of useful properties, including variable surface shape, amplified surface area, and overall surface function. (Conte et al., 2019). Moreover, possible uses of electrospun nanofibers incorporate tissue designing, filtration, optical gadgets, sensors, wound mending, catalysis, materials, tranquilize gracefully, and energy abstraction (Conte et al., 2019).

Chapter 3

METHODOLOGY

Chemicals i.e. Polyvinylidene fluoride (99% AR) in powder form, The polymer has a simple chemical formula-(CH2-CF2)-and can crystallize in at least four crystal phases called α, β, γ, and δ. (Costa et al., 2010). The vapour pressure of polymer was 15 mmHg at 32℃ with average molecular weight ~534000 and organic solvents Acetone and Dimethylformamide (DMF) were purchased from Sigma Aldrich and Daejung Korea respectively.

3.1. Different organic film depositions techniques:

There are different organic film depositions techniques used in the organic polymers to deposit on the substrate.

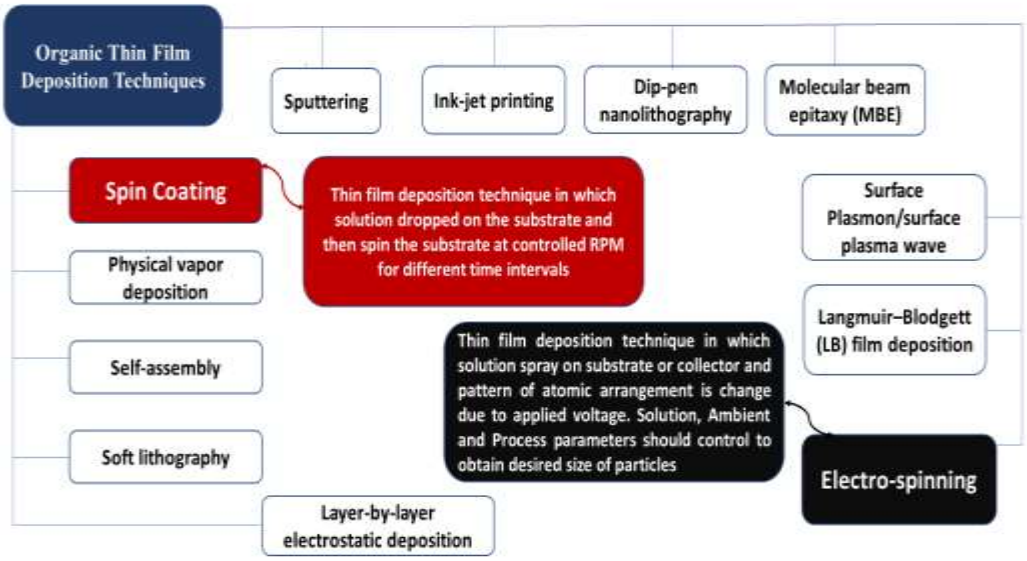

Figure 3.1 Different organic film depositions techniques used in the organic polymers

3.1.1. Spin Coating:

Spin coating is a modest method for rapidly depositing thin layers onto comparatively smooth substrates. Utilize some rotatable apparatuses to fix the substrate to be secured (typically utilize a vacuum to settle the substrate on set up), and afterward convey the layer arrangement onto the surface; the impact of the revolt is to spread the solution and leave it on the outside of the substrate very uniform layer of chosen materials. The spin coating process has been extensively researched in the past, and the information on the factors controlling the coating aggregate and the final thickness of the final aggregate is very good (Krebs, 2009).

3.1.1.1. Solution preparation for spin coating:

Table 3.1: Solution preparation of different concentration for spin coating

Sr. No.	% wt./v of PVDF in 10 cm^3 of DMF/Acetone	Procedure (at Stirring 600~800 RPM and heating 60°C)
F_1^{SC}	8% 0.8 g of PVDF	Dissolve the 0.8 g of PVDF in DMF/Acetone binary solution with fixed wt. % of 7:3. Stirring and heating the solution for 24 h. Finally, spin-coated on the substrate
F_2^{SC}	10% 1g of PVDF	Dissolve the 1g of PVDF in 10 ml of DMF/Acetone binary solution with fixed wt. % of 7:3, stirring and heating the solution for 24 h. Finally, spin-coated on the substrate
F_3^{SC}	12% 1.2g of PVDF	Dissolve the 1 g of PVDF in 10 ml of DMF/Acetone binary solution with fixed wt. % of 7:3, stirring and heating the solution for 24 h. Finally, spin-coated on the substrate
F_4^{SC}	12% 1.2 g of PVDF with 1% Carbon Black a source of Carbon to make the thin film more adhesive on the substrate and active w.r.t. light absorbance	Dissolve the 1.2 g of PVDF in 10 ml of DMF/Acetone binary solution with fixed wt. % of 7:3, stirring and heating the solution for 24 h. Finally, spin-coated on the substrate

Figure 3.2: Stirring of the solution on a hot plate at control temperature and RPM

3.1.2. Electrospinning:

Electrospinning is a very inexpensive fast and manageable method (Matabola & Moutloali, 2013), which currently its initial stages in industrial production (Matabola & Moutloali, 2013). Under varying conditions, the resulting fibres produced have different diameters Applied voltage can cause the spherical droplet into a Taylor cone and an ultrafine nanofiber in to at critical voltage

The electrospinning process consists of various steps:

a. Apply a strong electric field between the conductive substrate and the polymer solution present in the nozzle
b. When the voltage influences at the optimal value, the electrostatic force overcomes the surface tension of the solution
c. Charged solution droplets are ejected from the nozzle and then sprayed on the substrate in a dry environment (inside the instrument)
d. Finally, the dried droplets or jets are collected on the substrate to form a film composed of particles or fibers

Table 3.2: Conditions which can affect the synthesis of fibres are

PARAMETERS	
Solutions parameters	Concentration of solution vapour pressure of Solvent
Ambient conditions	Temperature, Humidity within the Electrospinning instrument
Process parameters	Distance from the nozzle to substrate applied voltages

By controlling these above parameters, the diameter of produce will be different (Wang, Zheng, Ren, Zhang, & Xu, 2011).

3.1.2.1. Solution preparation for Electrospinning:

Solution preparation has a significant effect on the electrospinning process. According to previous research and literature review, the minimum quantity of polymer is required for fibres generation is 8% wt./wt. (Beachley & Wen, 2009) and (Costa et al., 2010). So, we started our first trail to make proper fibres of a solution with 8% wt./wt. the concentration of PVDF. To achieve the first objective of the research following methods were used to prepare different concentration of solutions.

Figure 3.3: Homogeneous Solution of PVDF Pallets and DMF/Acetone

Table 3.3: Preparation of solutions of different concentration for Electrospinning

Sr. No.	% wt./v of PVDF in 10 ml of DMF/Acetone	Procedure (at Stirring 600~1000 RPM and heating 60°C)
$\mathbf{F_5}^{ES}$	8% 0.8g of PVDF	Dissolve the 0.8 g of PVDF in 10 ml of DMF/Acetone binary solution with fixed wt. % of 7:3, stirring and heating the solution for 24 h. Finally, electrospun on the substrate
$\mathbf{F_6}^{ES}$	10% 1g of PVDF	Dissolve the 1g of PVDF in 10 ml of DMF/Acetone binary solution with fixed wt. % of 7:3, stirring and heating the solution for 24 h. Finally, electrospun on the substrate
$\mathbf{F_7}^{ES}$	12% 1.2 g of PVDF	Dissolve the 1.2 g of PVDF in 10 ml of DMF/Acetone binary solution with fixed wt. % of 7:3, stirring and heating the solution for 24 h. Finally, electrospun on the substrate
$\mathbf{F_8}^{ES}$	15% 1.5 g of PVDF	Dissolve the 1.5 g of PVDF in 10 ml of DMF/Acetone binary solution with fixed wt. % of 7:3, stirring and heating the solution for 24 h. Finally, electrospun on the substrate

3.1.2.2. Ambient Conditions

There are two major factors which affect the formation of nanofibers during the electrospinning procedure

a) Temperature,
b) Humidity within the Electrospinning instrument

3.1.2.3. Procedure Parameters:

Cleaning of the substrate with Acetone followed by 2-Isopropanol for 10 minutes each. Then Ethanol and D.I. water and dry with hot air dryer to make sure the surface is properly cleaned and avoid the chances of contamination. The flow rate was adjusted to 2000-10,000 micron liter per hour depending on the viscosity of different solutions. The applied voltage in electrospinning was 15~18 kilovolts. at room temperature and film collected directly on substrate in a horizontal electrospinning setup.

Figure 3.4: Cleaning of Substrate with 2.Isopropanol and Acetone

The systematic scheme of instrument used in the electrospraying and electrospinning process is shown in Figure 3.5. Use a 20 ml glass syringe and a steel needle with an inner diameter of 0.34 mm. Use a Botanica Fluidentica L10 (0-30 kV) high-voltage power supply, the distance among the needle and collector is 10-12 cm, applied voltage is 15-18 kV. The collector used was an glass substrate with a thickness of 1 µm and a width of 1 cm. The process is carried out under the conditions of 25°C and 55% relative humidity.

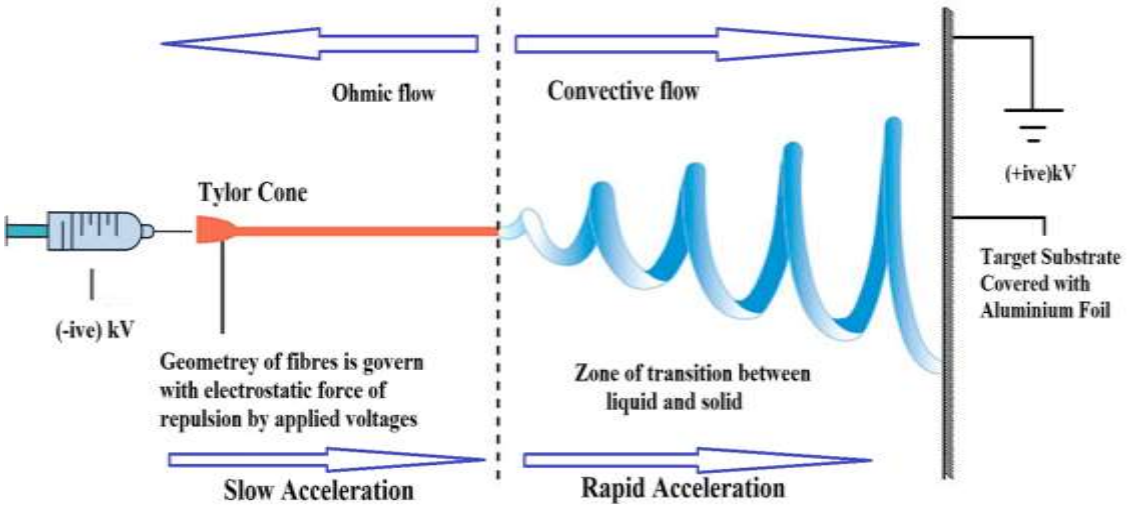

Figure 3.5 Schematic diagram of the electrospinning process

The schematic above shows the electrospinning process, depositing nanofibers of the solution on the FTO glass substrate. Cover the 0.5 cm glass substrate with transparent tape to prevent the film from being exposed and stick the electrode directly. After film deposition, these substrates were vacuum oven dried.

3.2. Characterization techniques of thin films and nanofibers:

To characterize these thin films and nano-fibres samples were analyzed with different techniques i.e. FTIR, XRD, UV-VIS-Spectroscopy, Hall-Effect and SEM.

3.2.1. Working of SEM:

The SEM mechanism involves the following components:

a. The source that produces high-energy electrons is called an electron gun, as in Fig 1.
b. Tilt down to pass electrons through two or more electromagnetic lenses, as in Fig 2.
c. The deflection system consists of scanning coils.
d. The electron detector is used for backscattering and secondary electrons, as in Fig 3.
e. The sample chamber is as in Fig. 4.

f. A computer system includes a observing screen to display the scanned photos, and a keyboard to regulate the electron beam.

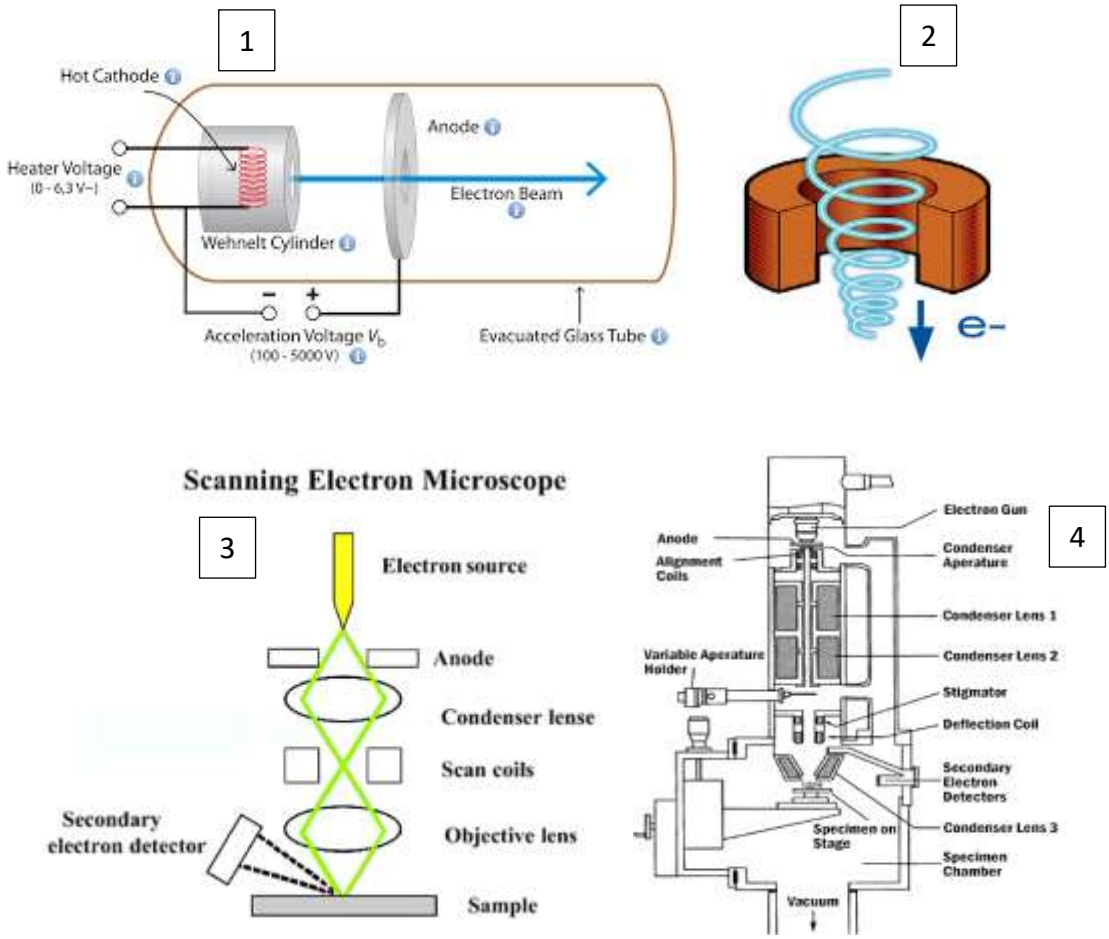

Figure 3.6: Schematic diagram of SEM (Ni, 2013)

3.2.2. Working Principle of FTIR:

Achieving Infrared Spectrum In various practical devices, the Fourier Transform Infrared (FTIR) spectrophotometer is the most widely used.

Common test procedures are as follows:

a. **The Source:**

Infrared rays are discharged from a source. The beam of radiations permits through a hole that regulate the energy providing to the sample (and eventually to the sensor).

b. **The Interferometer:**

The beam enters the interferometer where the "spectral information" occurs. The generated interferogram signal then leaves the interferometer.

c. **The Sample:**

The light beam enters the sample compartment dependent on the type of investigation to be performed where it is diffused or imitated from the sample surface. Now, a certain frequency of energy is immersed, which is a unique feature of the sample.

d. **The Detector:**

The beam finally passes through the sensor for final measurement. Use detector Inter-frame diagram dedicated to measuring signals.

e. **The Computer:**

The measured range is converted into electrical signal and sent to the computer for Fourier transform. Then present the final spectrum to the user for interpretation and further operations.

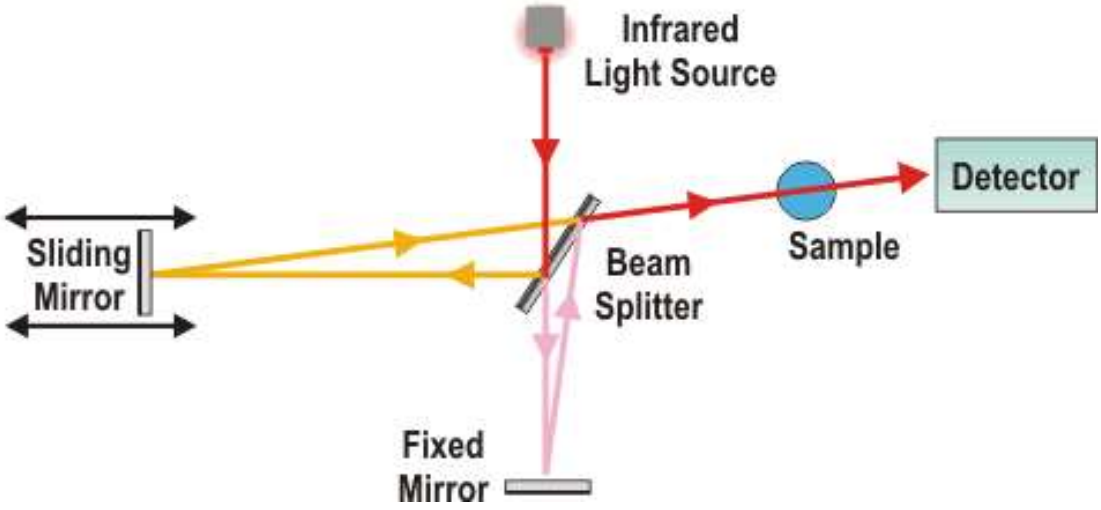

Figure 3.7: Schematic diagram of FTIR (instrumentationforum)

3.2.3. X-Ray Diffraction Analysis:

X-ray diffraction is an important technique for the investigation of nature of matter. Differential experimentations using X-rays help to examine the structural properties of nuclear-grade materials. This technique is also used to measure the crystallite size and determine the tensile strength, chemical composition, order state and phase diagram.

3.2.3.1. Working Principle of XRD:

The crystalline substance acts as a three-dimensional diffraction grating at the X-ray wavelength, comparable to the spacing of crystal planes in the lattice. X-rays interact with electrons in atoms and scatter elasticity. In the nuclear plane, many nuclear scattered waves can interfere with each other, and if the waves are in phase, they will cause constructive interference. These diffracted X-rays contain information about the distribution of electrons in the material

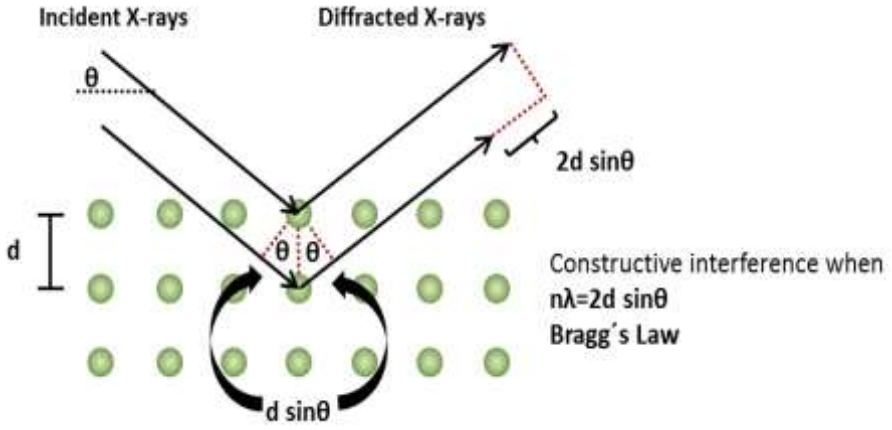

Figure 3.8 Working Principle of XRD (Antonxrd)

The diffracted beam is controlled by Bragg's law in a specific direction (θ), which relates the wavelength of the incident X-ray (λ) to the distance between the atomic planes (d) as,

$$2dsin\theta = n\lambda \qquad \text{EQUATION 0.1}$$

3.2.4. Working of UV-Vis Spectroscopy:

The absorption of ultraviolet and visible photons by molecules leads to the electronic excitation of the molecules, which is a characteristic of compounds. Electron transition involves the promotion of valence electrons from molecular orbitals from electronic ground state to high energy state called HOMO to LUMO.

These electronic transitions can be:

- **a.** Transitions relating π, σ, and *n* electrons
- **b.** Transitions relating charge - transmission electrons
- **c.** Transitions relating *d* and *f* electrons

1. A typical dual-beam ultraviolet-visible spectrophotometer is revealed in Figure 3.9. In a spectrophotometer, act as a light source (A mixture of deuterium lamps for ultraviolet range and tungsten lamps or halogen lamps for visible range) emits continuous radiation.
2. The beam separates its component wavelengths with different amplitudes through the grating.
3. A slit sends a narrow colored beam to the front of the spectrometer photometer.
4. Then, the light from the slit falls onto the rotating disc, which directs the light to the sample and reference cells, or by means of different parts of the disc.
5. The sample cell is filled with solution, the sample is dispersed or dissolved in it, and the reference cell is filled with pure solvent.
6. Through the cell, the second turntable transmits the light intensity to the detector.

7. The detector translates the intensity to the equivalent current signal, which is then read by the computer.
8. The computer compares the transmission intensity of the sample cell and the reference cell, and then uses,

$$A = log_{10} (I_0 / I) \qquad \text{Equation 0.2}$$

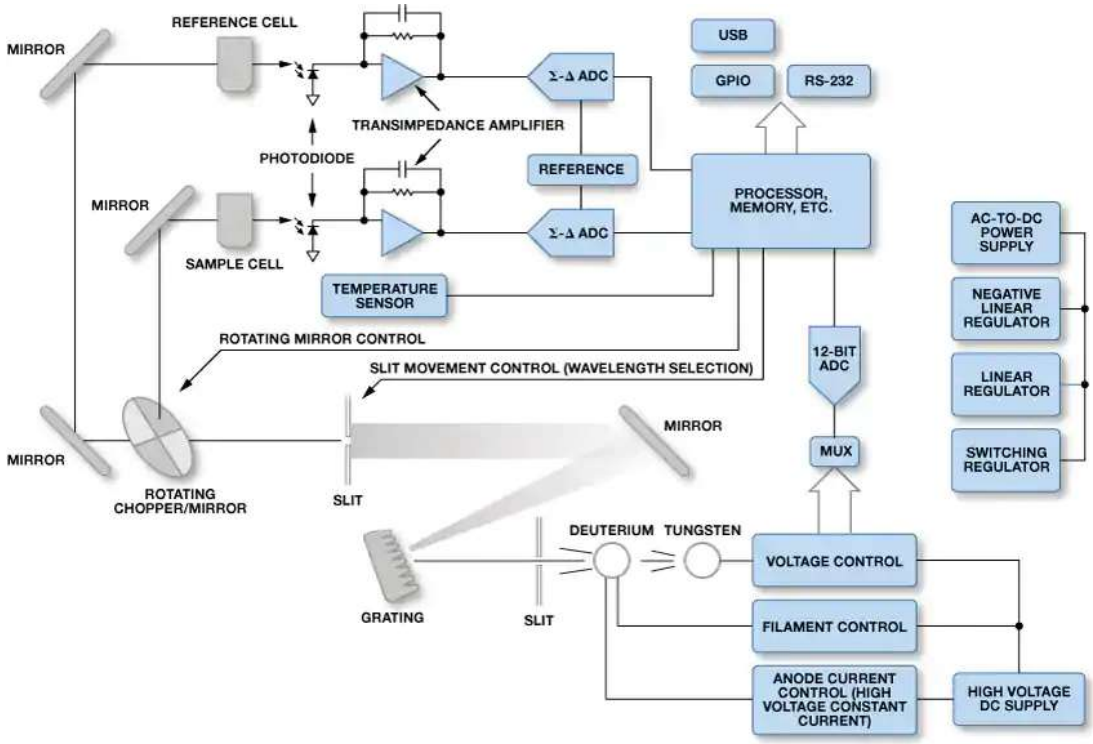

Figure 3.9: Dual Beam UIV-VIS Spectroscopy. (DIGI-KEY/product-highlight/a/analog-devices/chemical-analysis-and-environmental-monitoring#dual)

3.2.5. Working Principle of Hall-Effect:

Hall effect, when a solid material carries a current and is placed in a magnetic field perpendicular to the current, a transverse electric field is generated in the solid material. The electric field or Hall field generates force through a magnetic field which results in the movement of current and current positive and negative particles. Regardless of whether the current is a positive particle, the movement of a negative particle in the opposite direction, or a combination of both, the vertical magnetic field transfers dynamic charges in the same direction to the moving magnetic field and magnetic field direction. The magnetic field in the electric current.

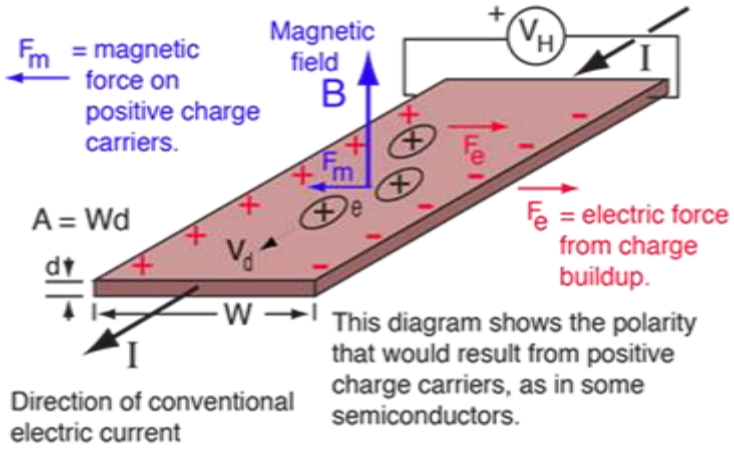

Figure 3.10 Working Principle of Hall-Effect ("Hall Effect History". Retrieved 2015-07-26.)

Accumulation of charge on one side of the conductor, on the other hand, causes opposing charges and makes a potential difference. Appropriate meters can detect this difference as positive or negative voltage. This hall voltage symbol determines whether a positive or negative charge is present.

The large magnetic field under Tesla's command is usually measured using the Hall effect. Place the thin-film Hall probe in a magnetic field and measure the lateral voltage (on the order of microvolts).

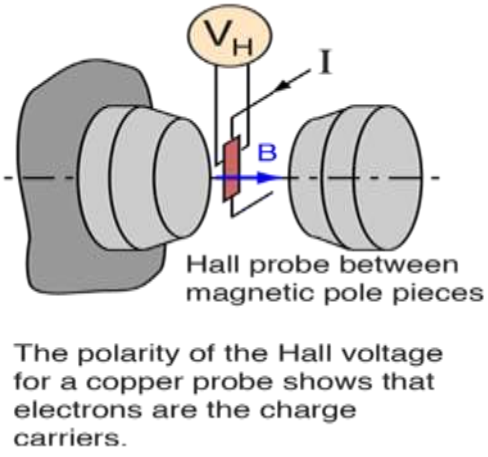

Figure 3.11: Hall probe ("Hall Effect History". Retrieved 2015-07-26.)

Sometimes a copper film with a thickness "d" of about 100 microns is used for the Hall probe. Taking the carrier density as

$$\mathbf{n = 8.47x\,10^{28}\ electrons/m^3} \qquad \textbf{EQUATION 0.3}$$

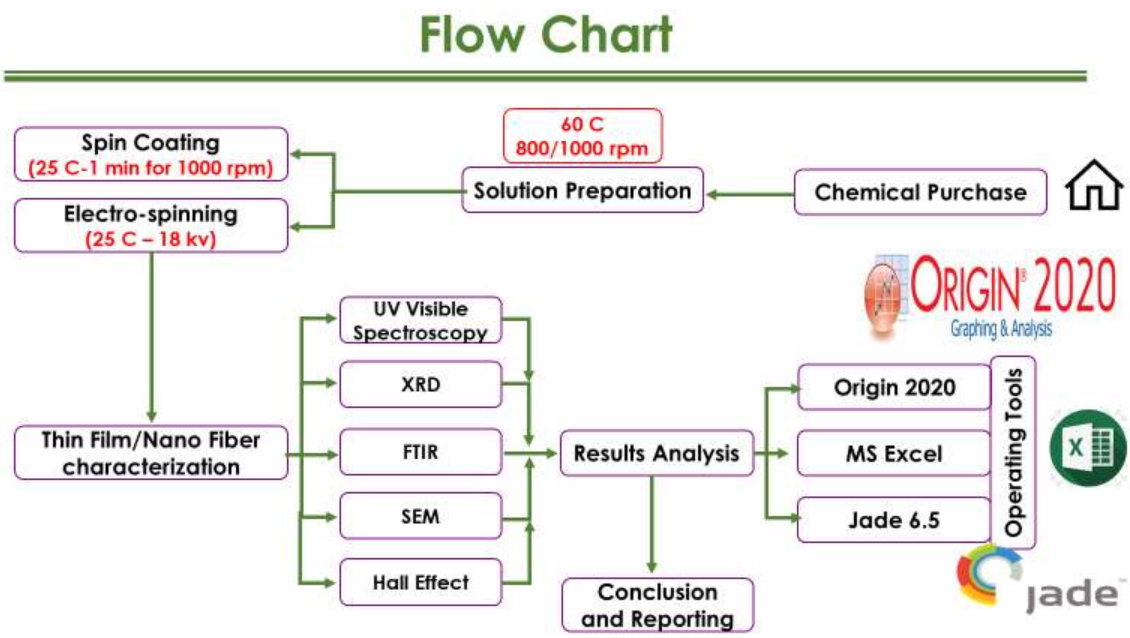

Figure 3.12 Flowchart of Methodology for Research Work

Chapter 4

RESULTS AND DISCUSSIONS

4.1. Characterization of Thin Films and Nano Fibers:

To characterize these thin films and nano-fibres samples were analyzed with different techniques i.e. FTIR, UV-VIS-Spectroscopy, XRD, Hall-Effect and SEM.

4.1.1. Morphological Characterization of Nano-Fibers:

Figure 4.1 shows a characteristic SEM image of PVDF nanofibers which gained from different concentrations of PVDF in an acetone/DMF binary solution. Adding more PVDF to the solution has a significant effect on fiber morphology. Fiber structure and size increase with PVDF material.

4.1.1.1. Structural characterization for 8% (w/w) PVDF:

The SEM results show that 8% concentration was not optimum for the nanofibers. Because the structure was very rough and not proper fibres. So, we will not take this concentration in our consideration to get nanofibers.

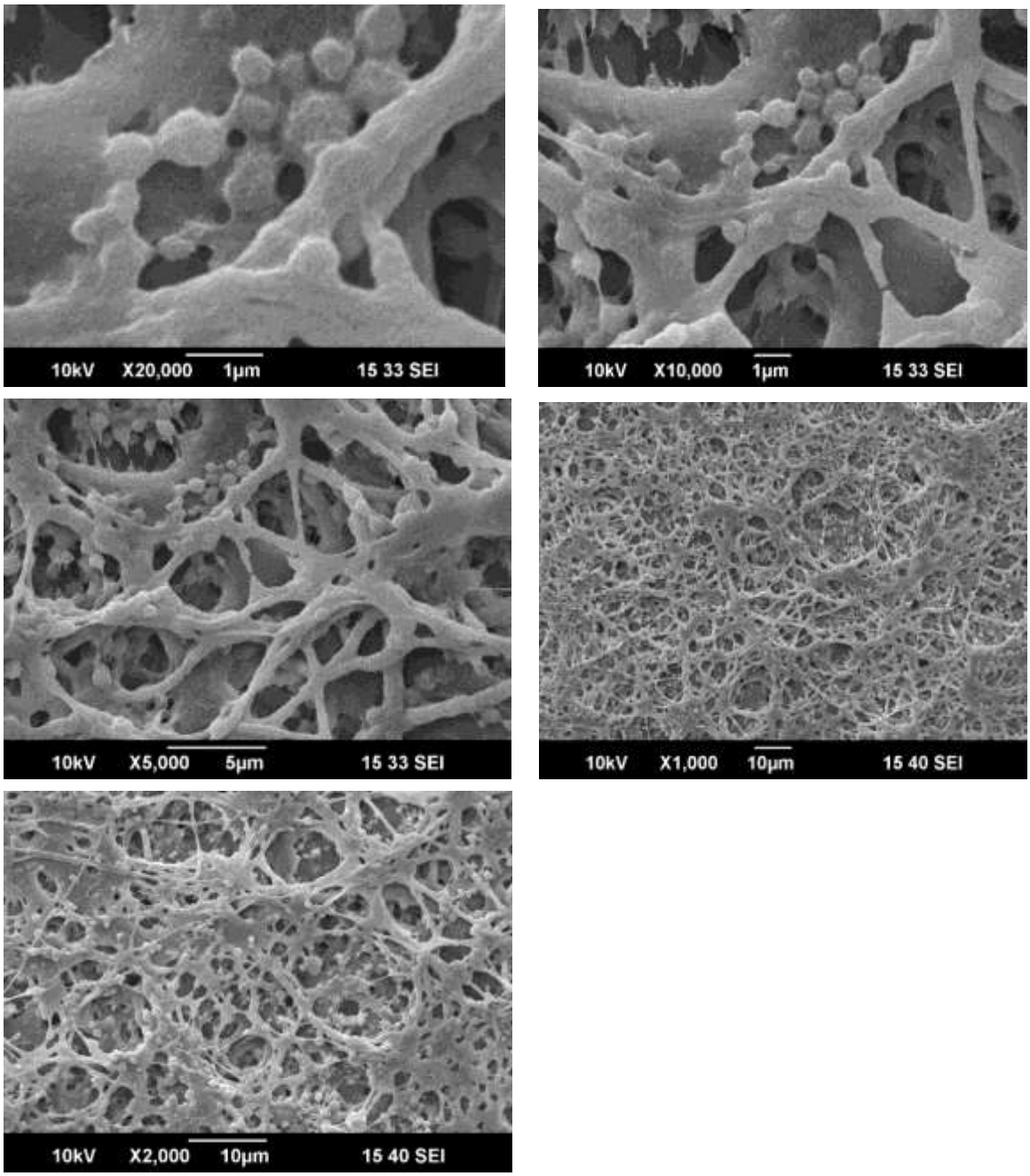

Figure 4.1: Structural characterization by SEM for 8% (w/w) PVDF

4.1.1.2. Structural characterization for 10% w/w PVDF:

On the concentration of 10% PVDF, we get the fine fibres with a diameter of 460.98 ~ 630 nanometers.

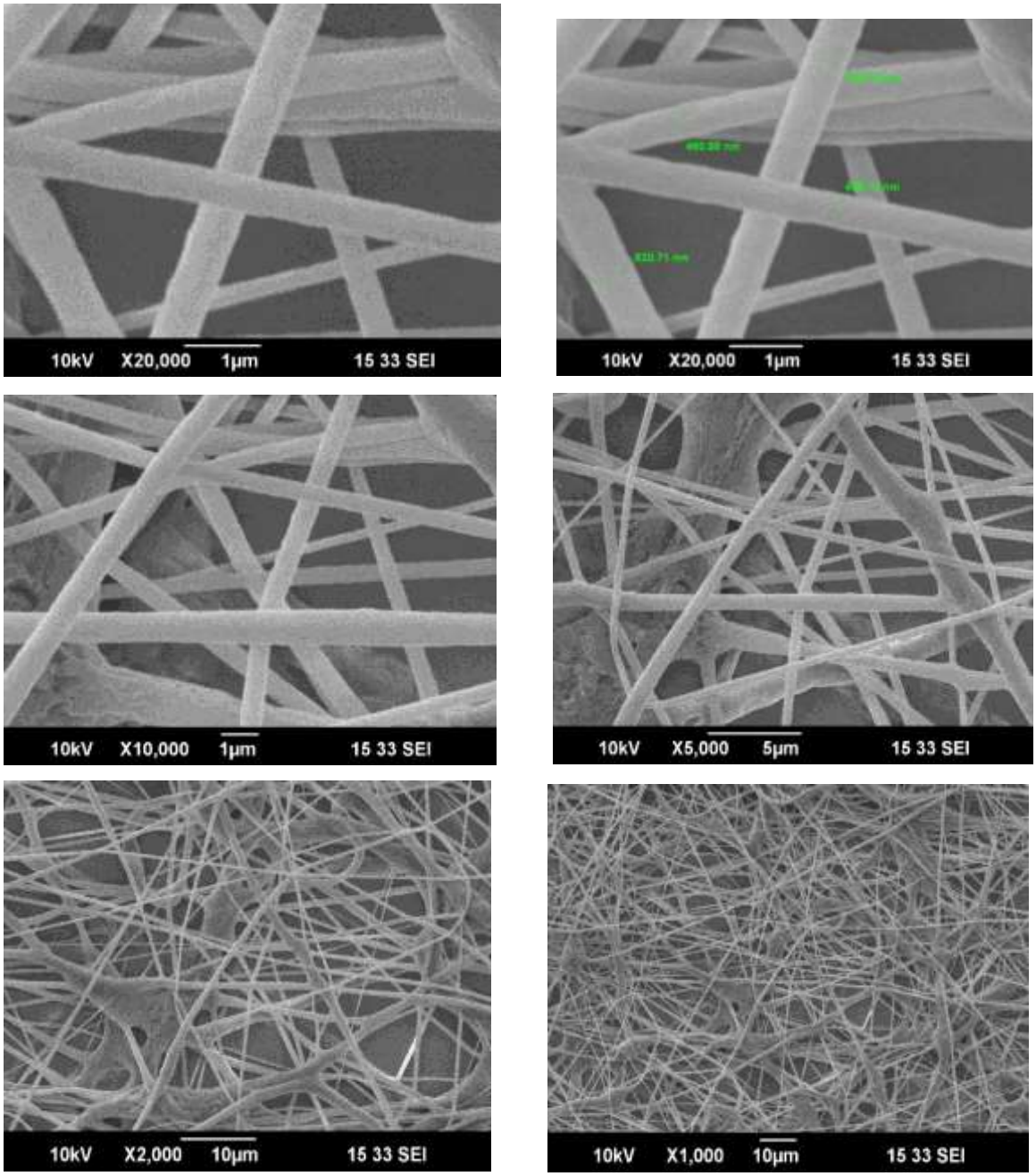

Figure 4.2: Structural characterization for 10% (w/w) PVDF

4.1.1.3. Structural characterization for 12 % w/w PVDF:

On the concentration of 12% PVDF, we get the fine fibres with a diameter of 259 nm ~ 644.13 nanometers.

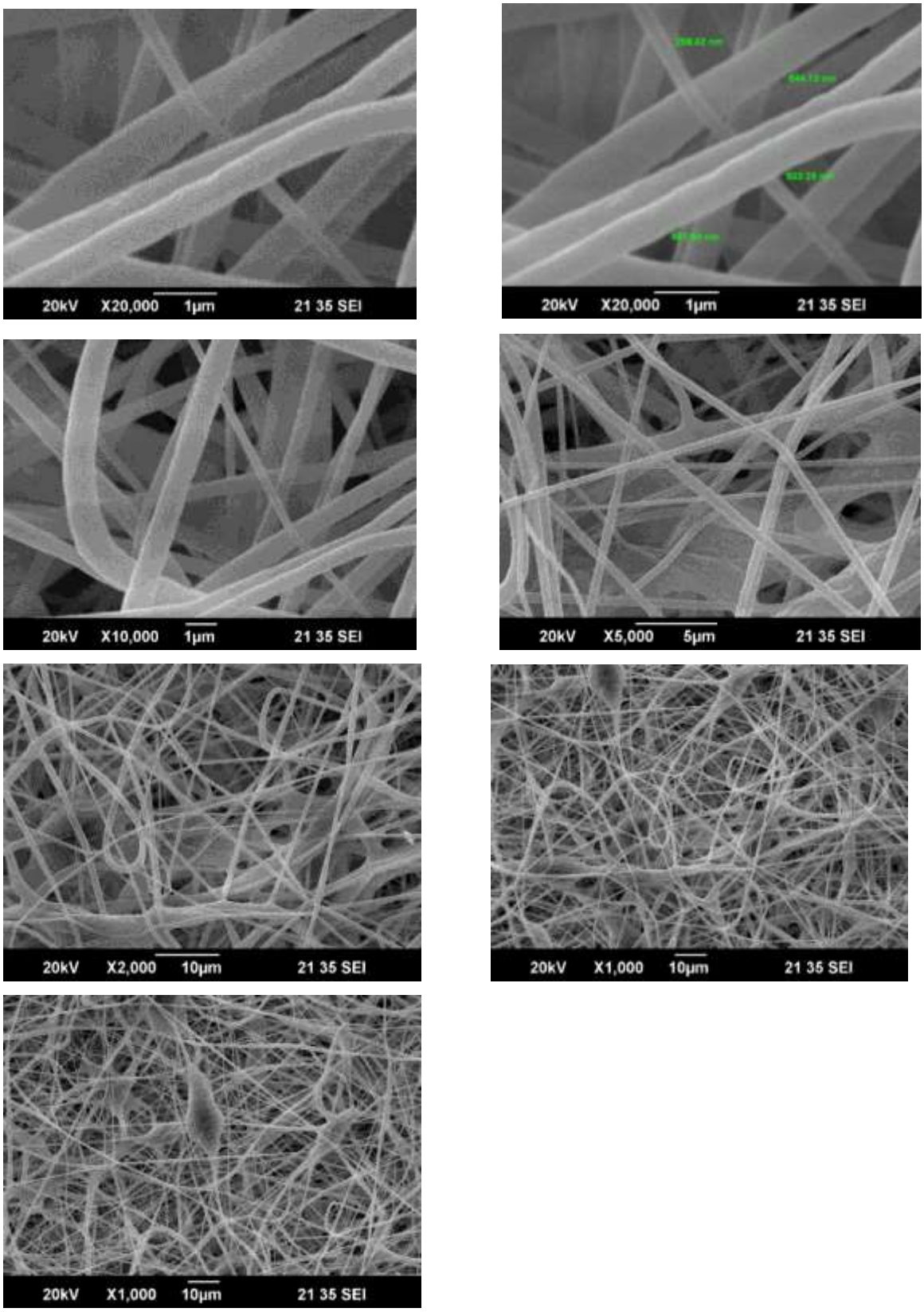

Figure 4.3: Structural characterization for 12% (w/w) PVDF

4.1.1.4. Structural characterization for 15% w/w PVDF:

The 15 % wt./wt. the concentration of PVDF shows fibres of large diameter and thickness was 261 ~ 636 nanometers.

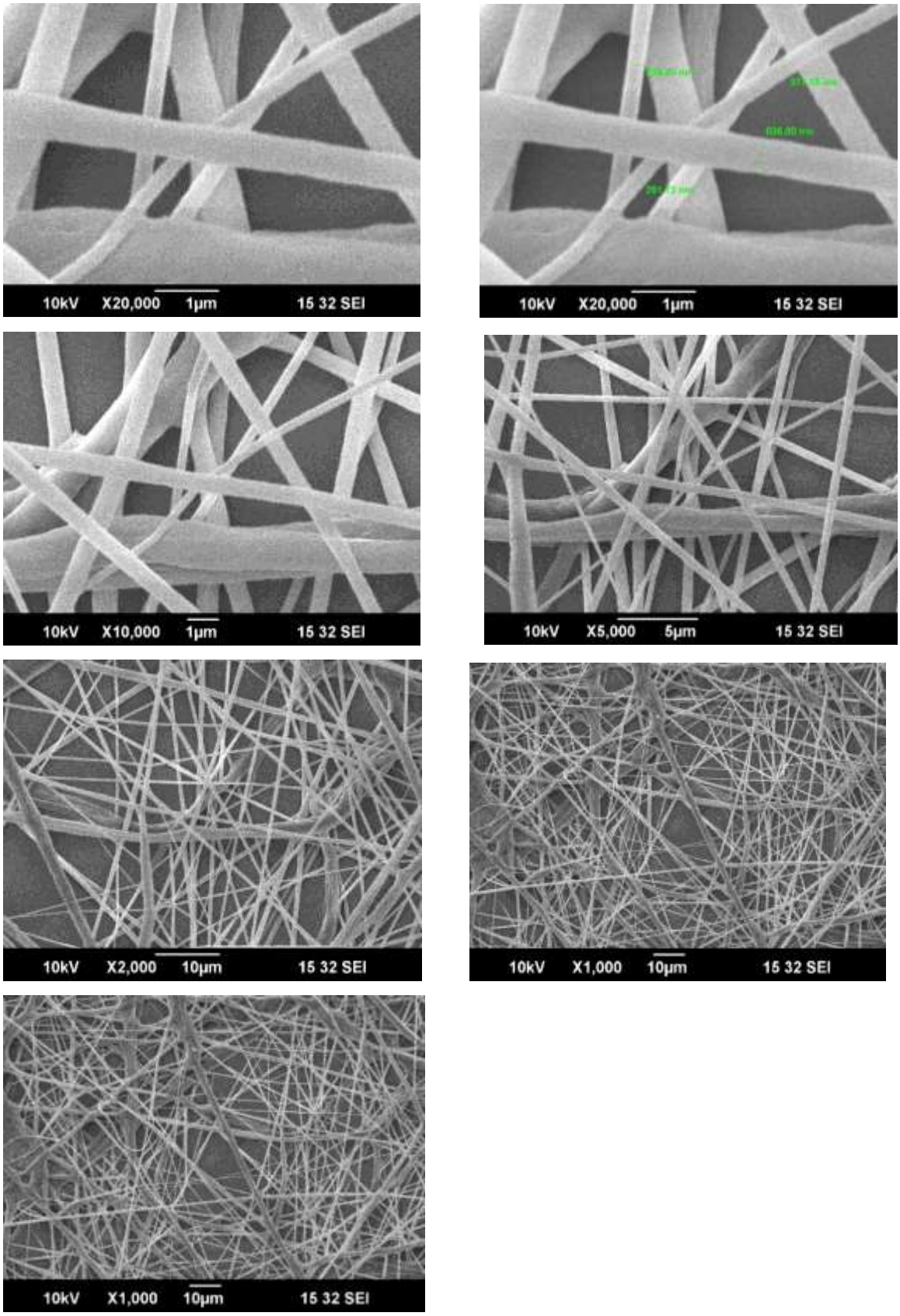

Figure 4.4: Structural characterization for 15% (w/w) PVDF

4.1.2. FTIR of Thin Films and Nano Fibers:

The FTIR results show that all samples of thin films and electrospun nanofibers contain β-phase the peaks assign to β-phase are at 840, 1071, 1176, 1234, 1401 are pure electroactive β-phase while the peak of 510, and 869 is the combination of beta and gamma phase (Cai, et al. 2017).

4.1.2.1. Integrated quantification of individual β and γ phase:

Three basic α, β, and γ crystals shapes of PVDF can be divided into three categories on the bases of the FTIR absorption peaks:

1. Common peaks (all three phases contain these common peaks)
2. Exclusive peaks (only phases have its own exclusive peaks)
3. Dual peaks (combination of two different phases of polymers)

Table 4.1: Assignment of some typical bands (Cai et al., 2017)

Wavenumber (cm^{-1})	**Crystalline Phase**
431	β γ β+γ
482	β γ α
510	β, γ, β+γ, α
840	β, γ, β+γ
881	β, γ, β+γ, α+β, α+β+γ, α
1071	β, β+γ, α+β+γ, α

1176	β, γ, β+γ
1234	β, γ, β+γ
1275	β, γ
1401	β, γ, β+γ, α

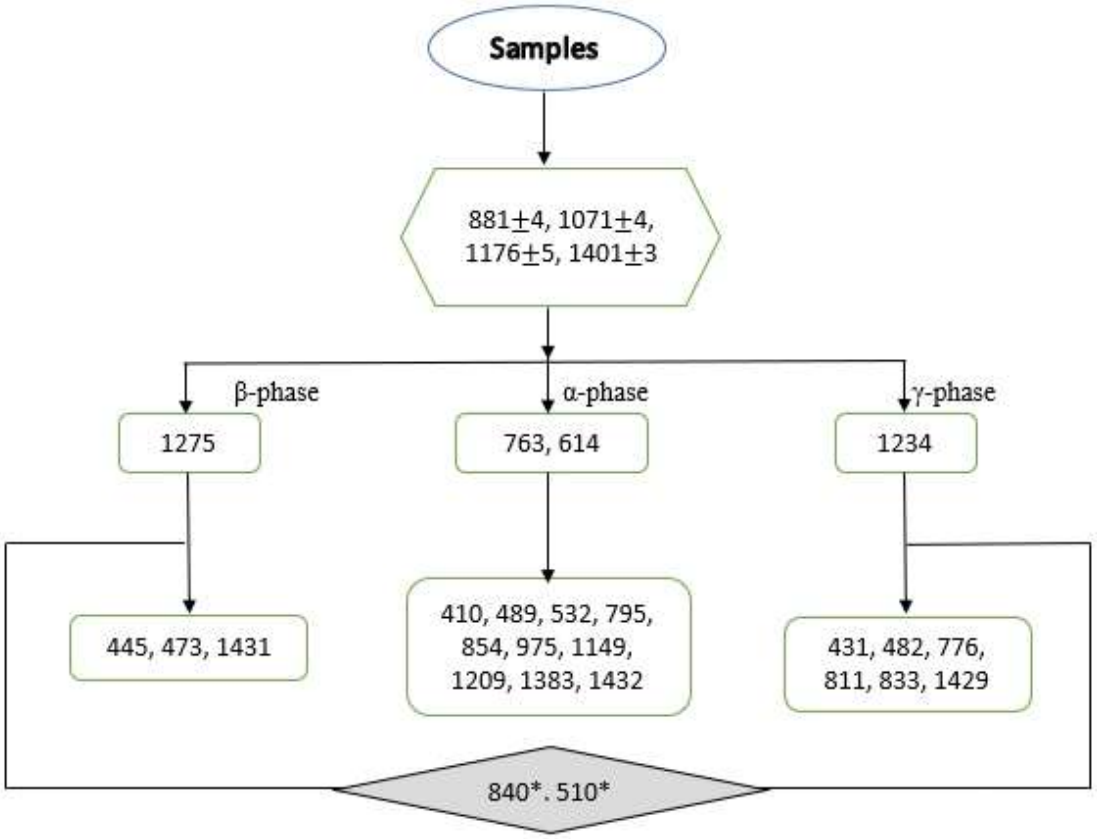

Figure 4.5: Flow diagram for the identification of phases

The α, β, and γ phases 840* and 510* represent the bands in the range of 837-841 and 508-512 cm-1, respectively. 776* and 833* reflect possible changes based on specific processes (Cai et al., 2017).

Since the 840*cm-1 frequency band can be allocated to β, γ or two phases based on the information of other frequency bands, each β and γ phase can be fully quantified (Cai et al., 2017).

The fraction of the crystalline components of the electrically active β phase and γ phase (FEA) in any sample, for example, containing only two phases (α+β, α+γ or β+γ) or three phases (α+β+γ), can be quantified as follows:

$$F_{EA} = \frac{I_{EA}}{\left(\frac{K_{840^*}}{K_{763}}\right) I_{763} + I_{EA}} \mathbf{x\,100} \qquad \textit{EQUATION 0.1}$$

Among them, I_{EA} and I_{763} are the absorbance at 840 * and 763 cm^{-1}, respectively; K_{840*} and K_{763} are the absorption coefficients of the corresponding wavenumbers, and their values are 7.7 x 10^4 and 6.1 x 10^4 cm^2 mol-1, respectively. From equation: when the 840* cm^{-1} frequency band is allocated to one of the electroactive phases, F_{EA} is undoubtedly equal to the relative score of the corresponding phase (Cai et al., 2017). Thus, below is to show how to quantify individual β and γ phases when the 840* cm^{-1} band is for both phases. The figure shows the FTIR spectra of spin-coated films and electrospun nanofibers using 8, 10, 12, 15 wt.% PVDF mixed with DMF/acetone. Using the above formula, we calculated the β phase of each sample shown in Table 4.1.

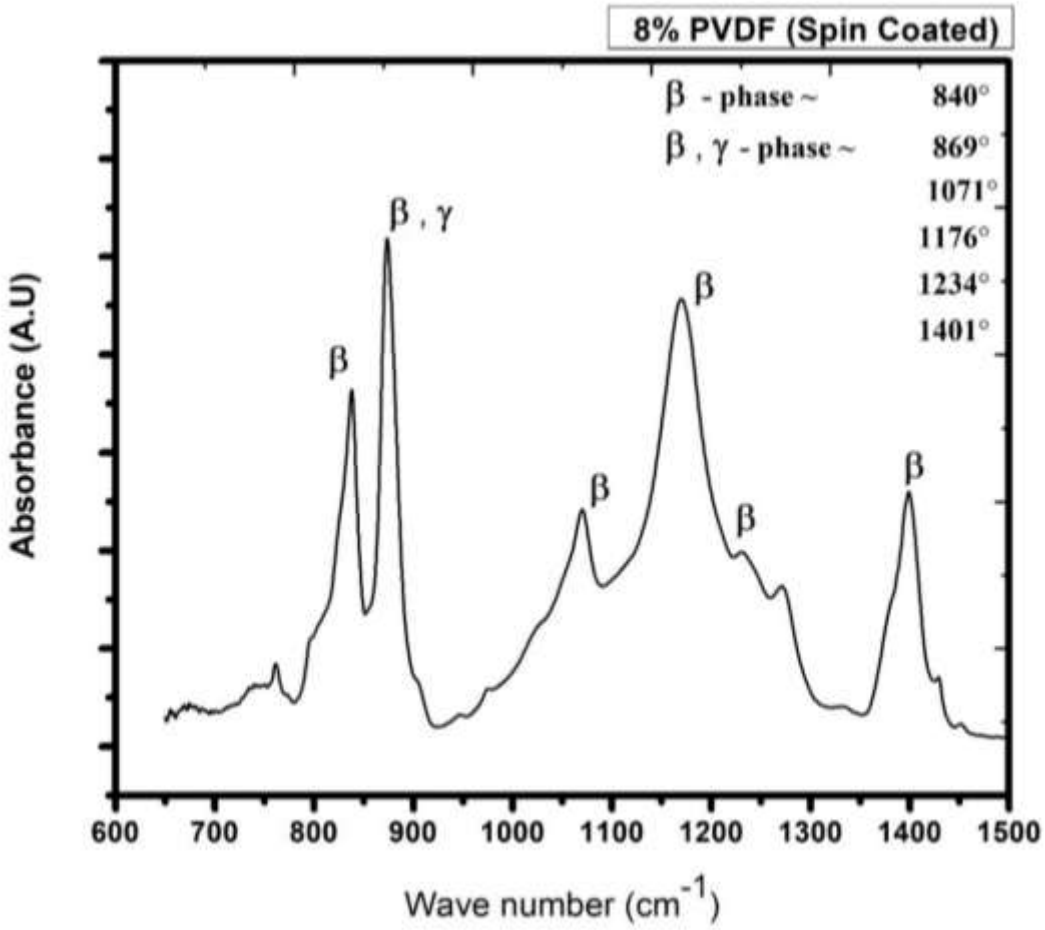

Figure 4.6: FTIR spectrum of the 8% PVDF solution (Spin-Coated thin-film)

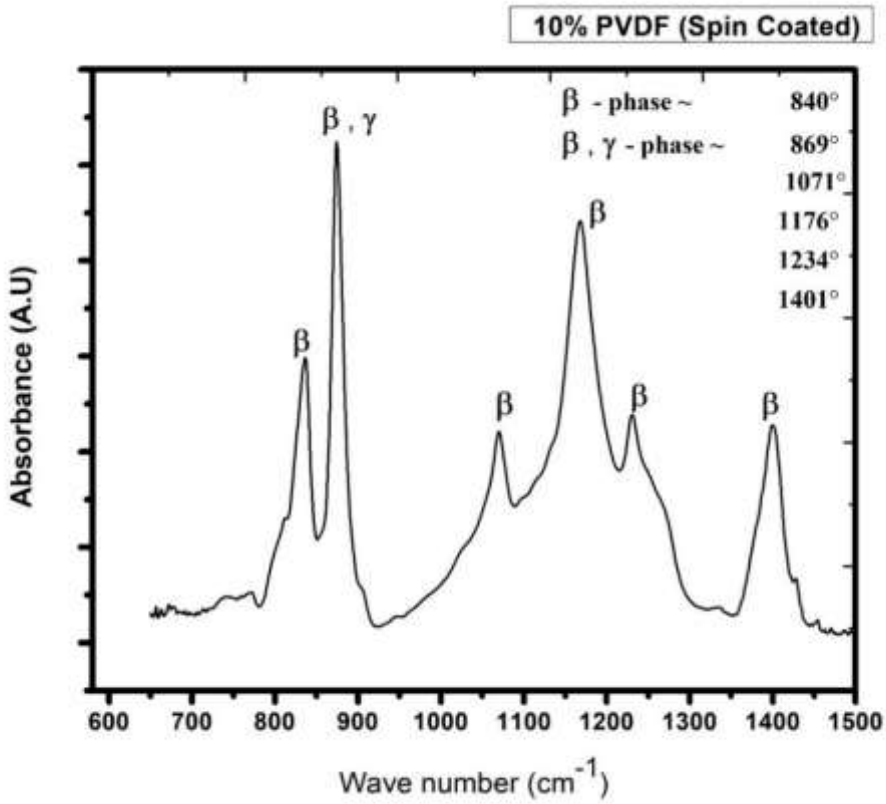

Figure 4.7: FTIR spectrum of the 10% PVDF solution (Spin-Coated thin-film)

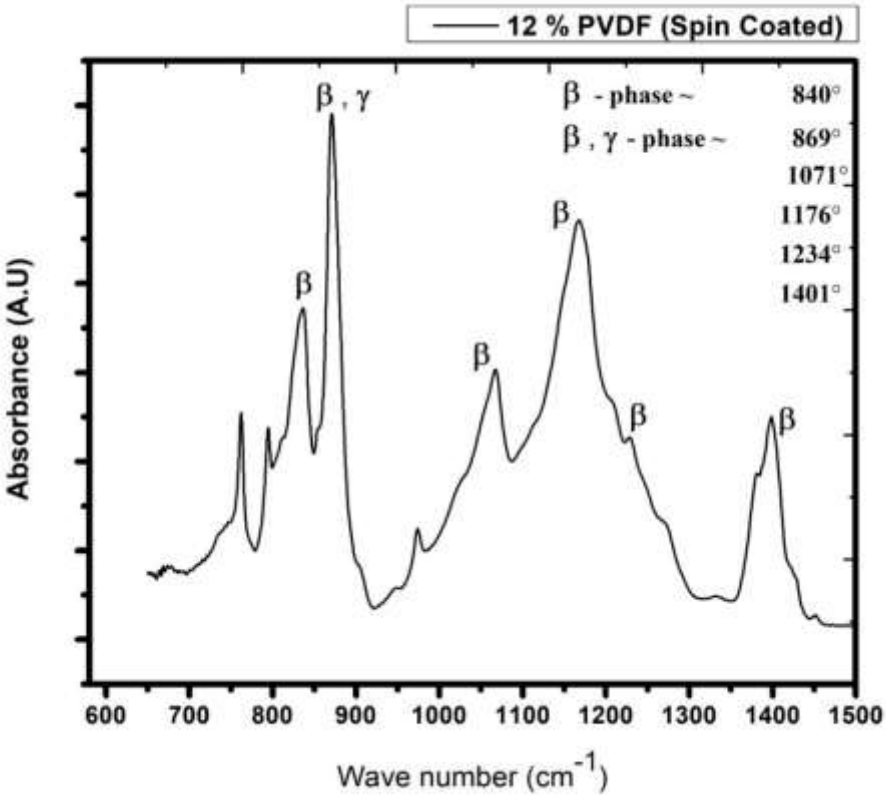

Figure 4.8: FTIR spectrum of the 12% PVDF solution (Spin-Coated thin-film)

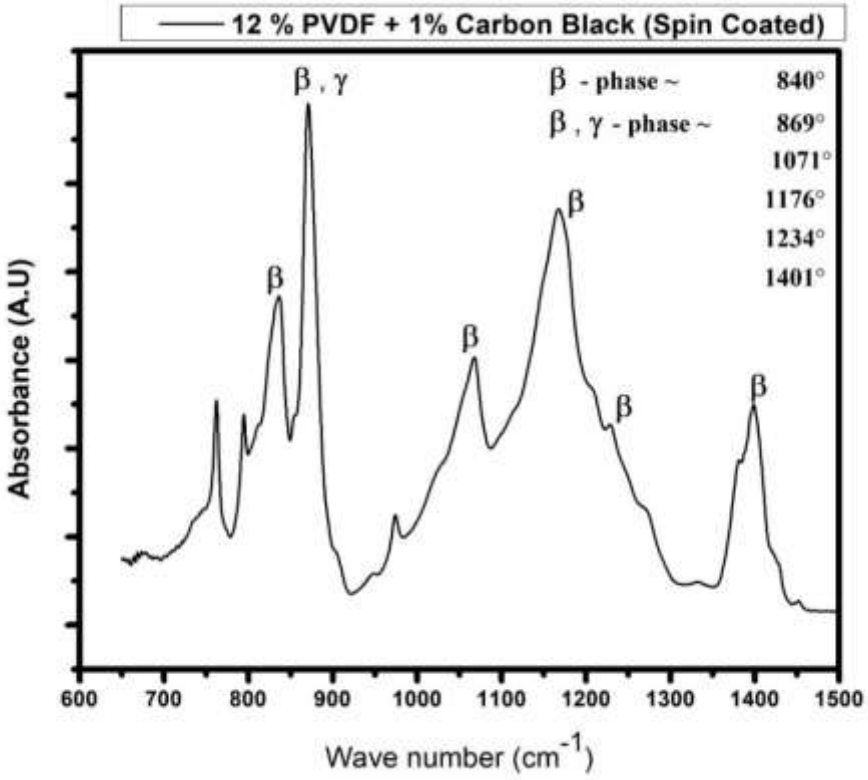

Figure 4.9: FTIR spectrum of the 12% PVDF doped with 1% Carbon Black solution (Spin-Coated thin-film)

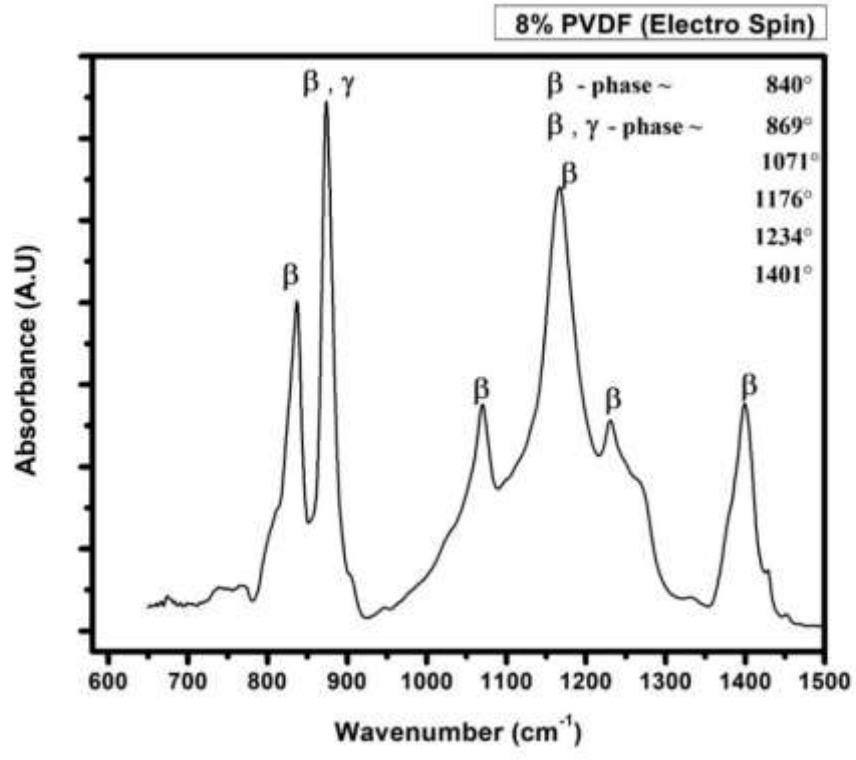

Figure 4.10: FTIR spectrum of the 8% PVDF Solution (Electro-spin Nanofibers)

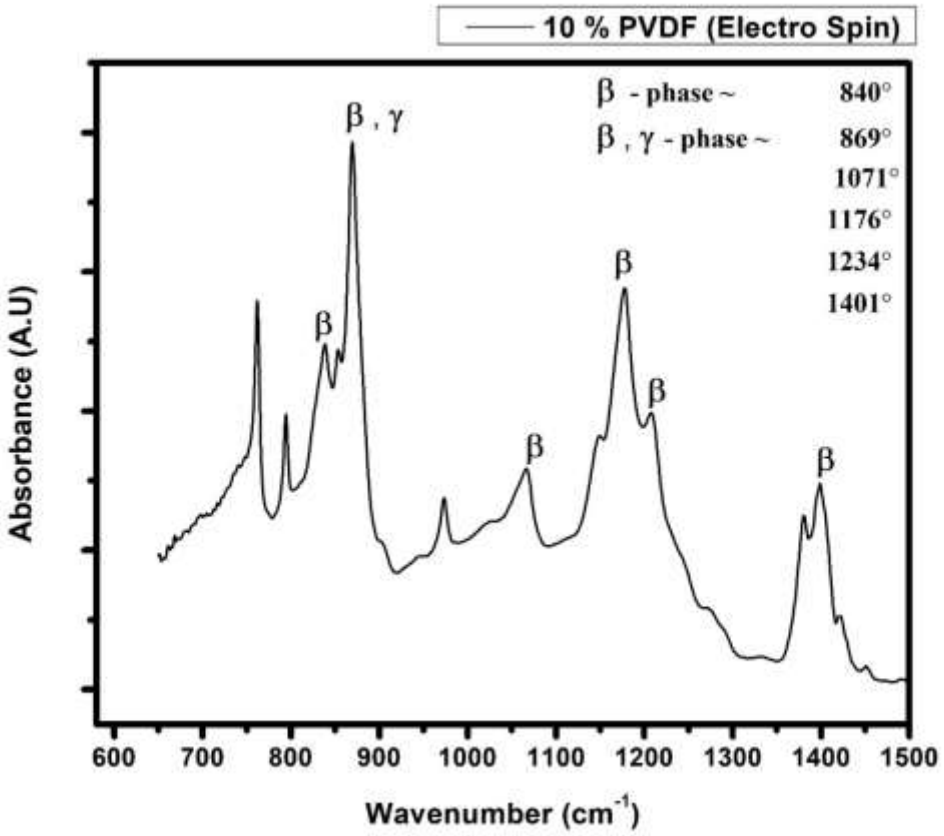

Figure 4.11: FTIR spectrum of the 10% PVDF Solution (Electro-spin Nanofibers)

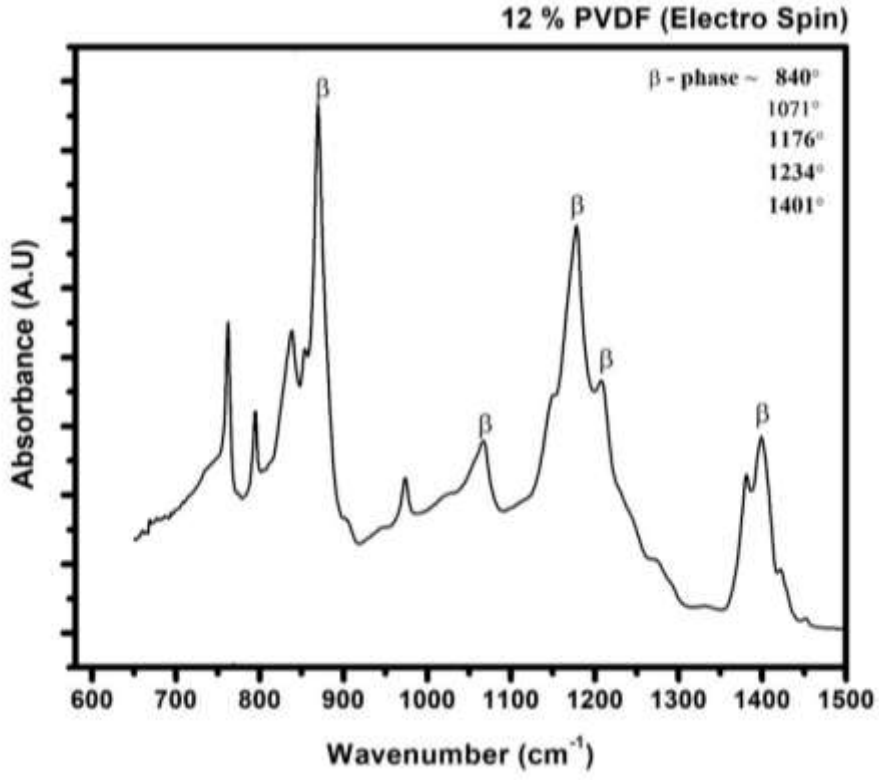

Figure 4.12: FTIR spectrum of the 12% PVDF Solution (Electro-spin Nanofibers)

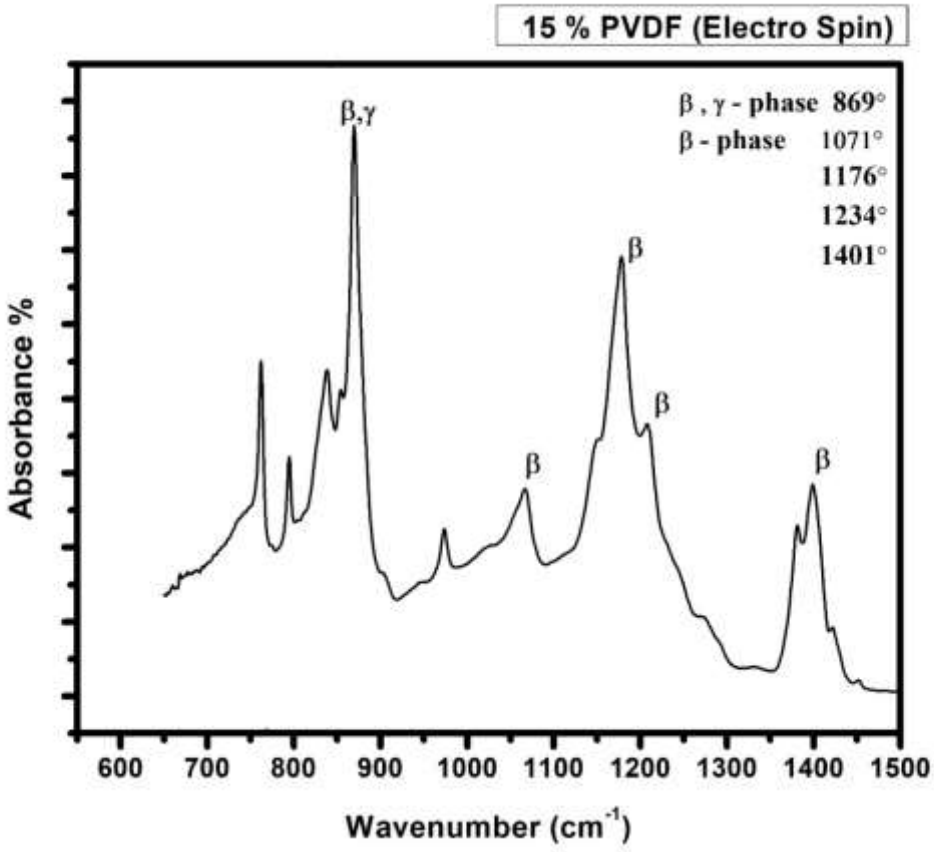

Figure 4.13: FTIR spectrum of the 15% PVDF Solution (Electro-spin Nanofibers)

By using the above equation, we calculated the β-phase of each sample shown in table 4.1.

Sr. No.	Sample Name	Fraction of β-phase (%)
1	F_1^{SC}	1.27
2	F_2^{SC}	1.18
3	F_3^{SC}	2.47
4	F_4^{SC}	7.68
5	F_5^{ES}	10.46
6	F_6^{ES}	16.12
7	F_7^{ES}	17.42
8	F_8^{ES}	12.42

Table 4.2: Integrated quantification of individual β and γ phase

By the above table, we can find easily that sample F_7^{ES} i.e. (12% PVDF and electrospun on the substrate) have the highest value of β-phase 17.42%.

4.1.3. XRD of Nano-Fibers and Thin-films:

The structural properties of polymer thinfilms and nanofibers were studied by X-ray powder diffraction. Analysis using Cu-K radiation (λ: 1.5406 A˚) using an X-ray diffractometer (PANalytical X'pert). The figure below shows the XRD pattern of PVDF pure electrospun nanofibers and spin-coated pure PVDF doped with carbon black film.

For polyvinylidene fluoride, it is well known that in typical PVDF samples, the crystal content does not exceed 50-60%. However, there is still no specific information on how the amorphous part of PVDF affects the XRD and IR spectra. (Cai et al., 2017).

In our research, the discussion is only concentrating on the crystalline phase, especially on the most common β-phase. Crystalline β-phase solid has the orthorhombic shape of crystal with the formula of $(C_2H_2F_2)_n$ at the angle of 2T=20.06° and 20.62° with (hkl value of 200 and 110) (Cai et al., 2017).

The results of XRD are as follows:

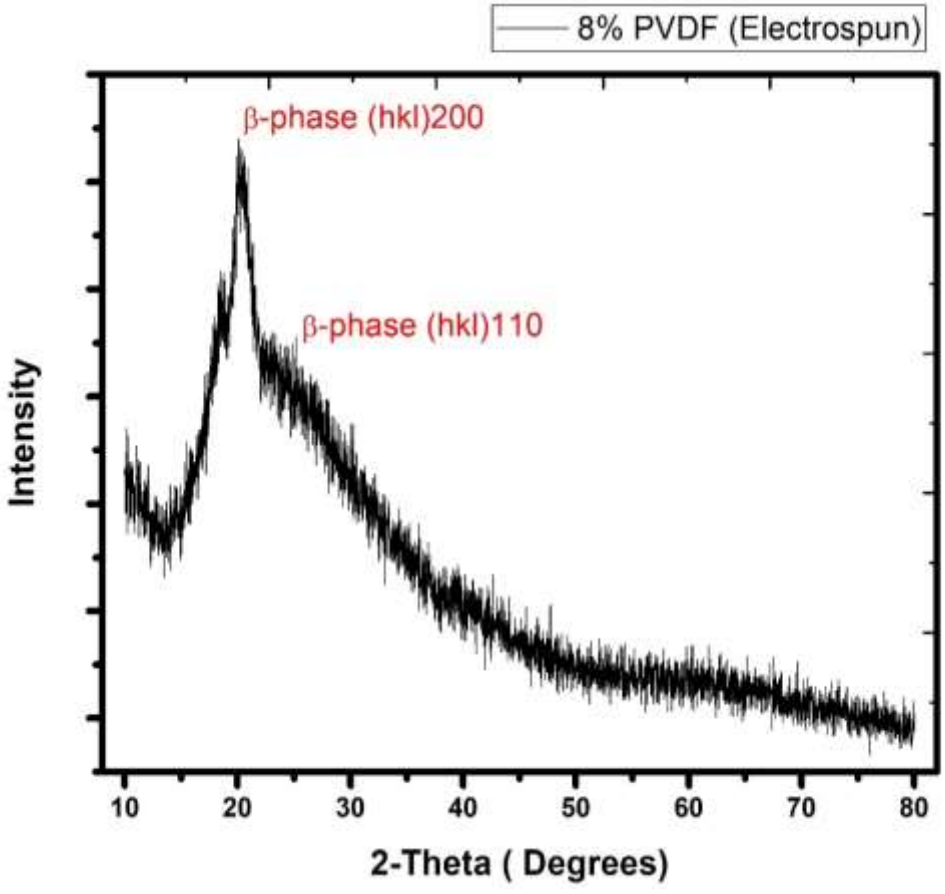

Figure 4.14: XRD pattern of the 8% PVDF solution (Electro-spin Nanofibers)

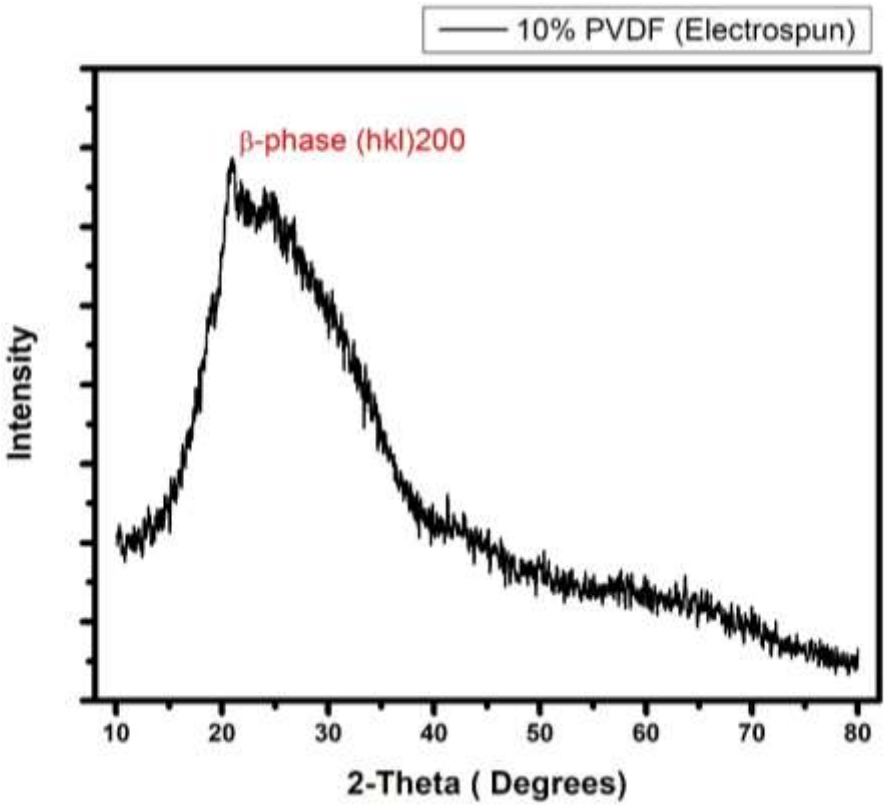

Figure 4.15: XRD pattern of the 10% PVDF solution (Electro-spin Nanofibers)

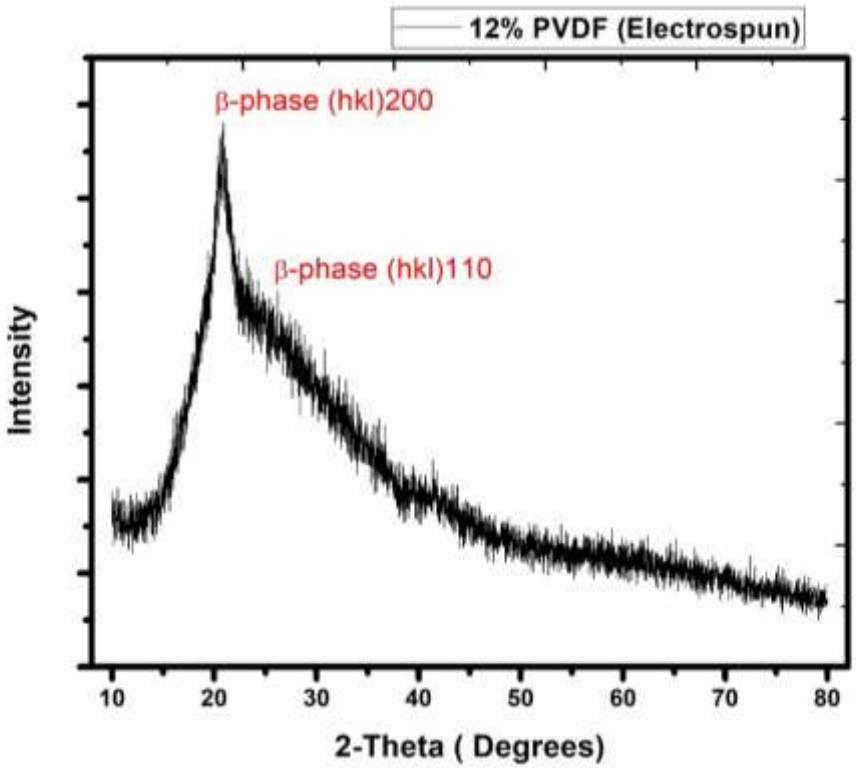

Figure 4.16: XRD pattern of the 12% PVDF solution (Electro-spin Nanofibers)

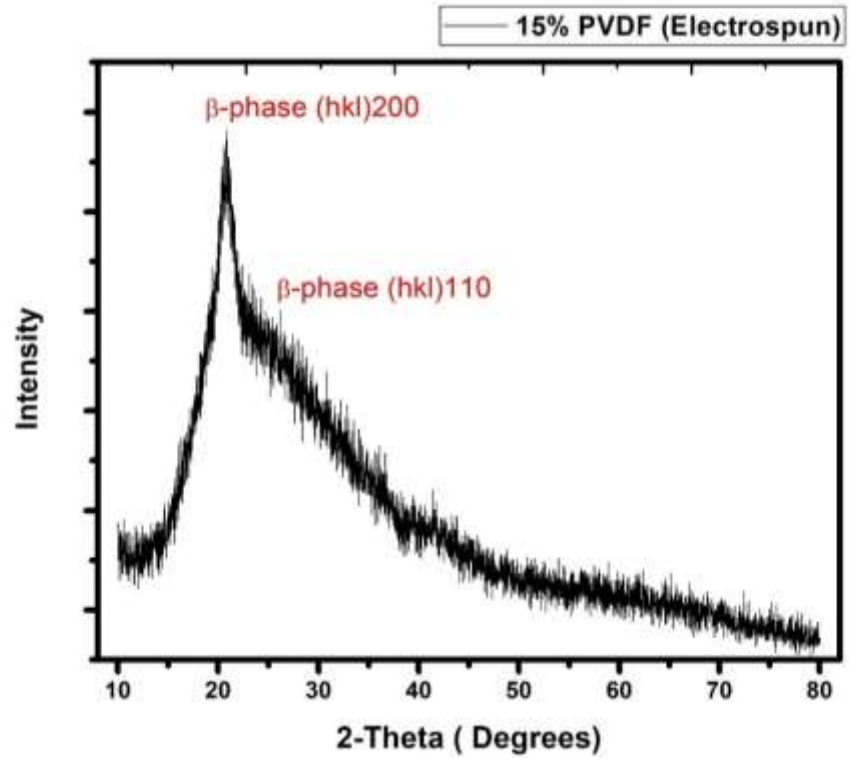

Figure 4.17: XRD pattern of the 15% PVDF solution (Electro-spin Nanofibers)

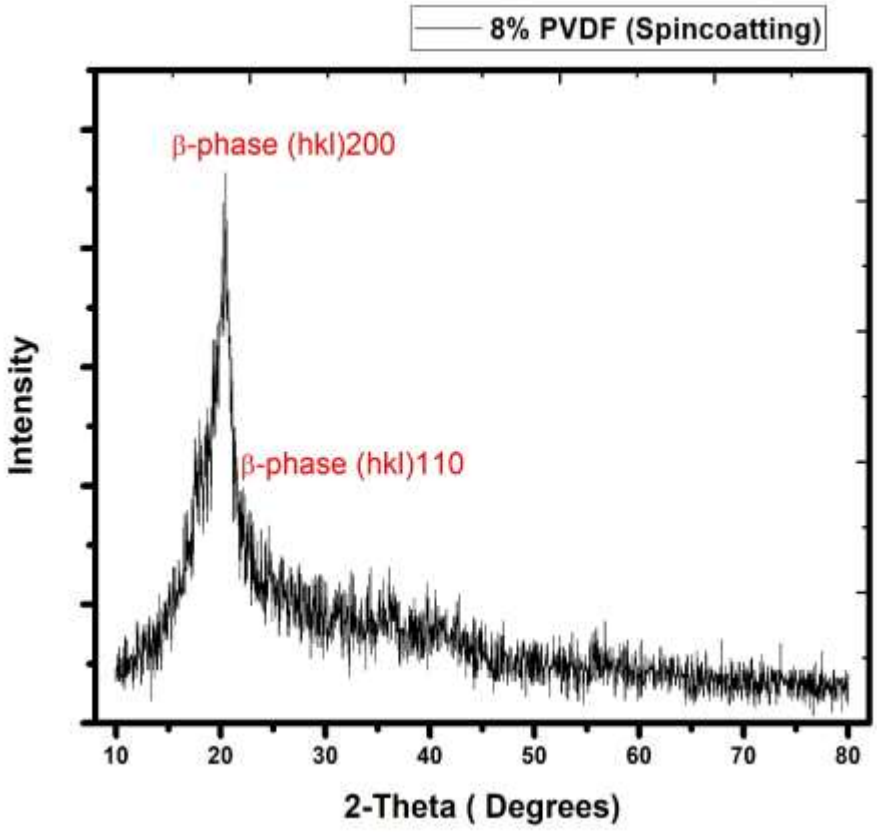

Figure 4.18: XRD pattern of the 8% PVDF solution (Spin-Coated thin-film)

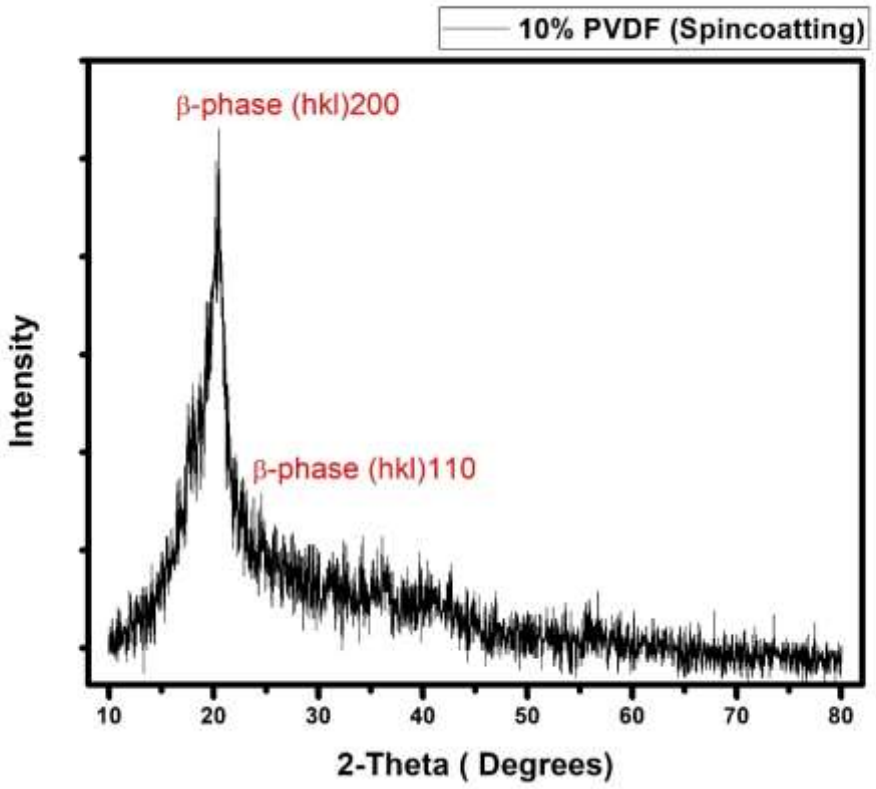

Figure 4.19: XRD pattern of the 10% PVDF solution (Spin-Coated thin-film)

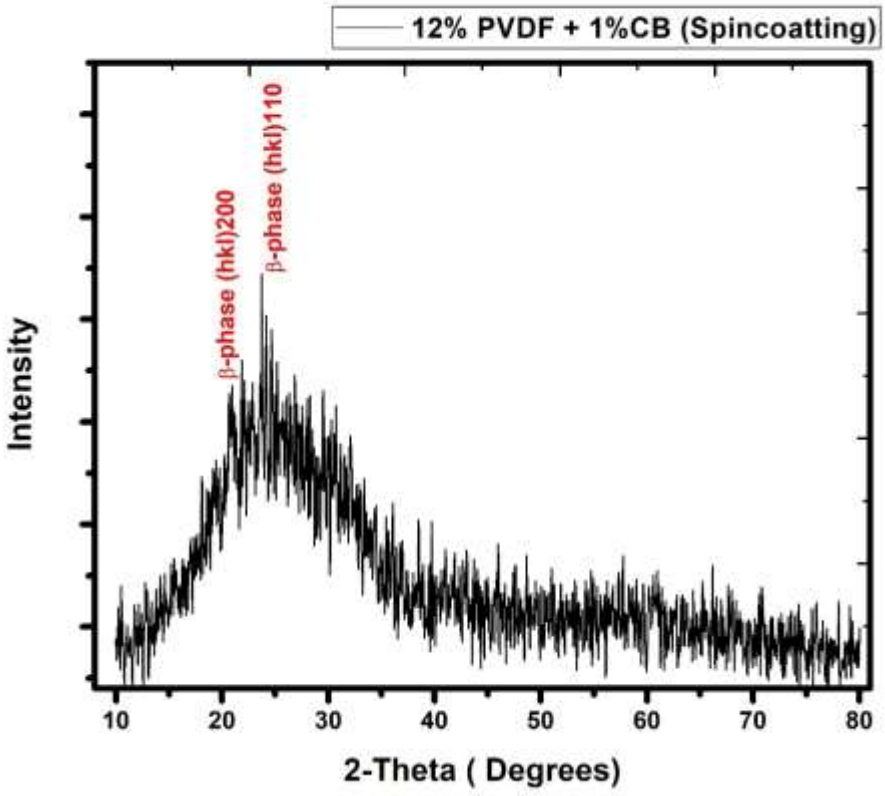

Figure 4.20: XRD pattern of the 12% PVDF doped with 1% Carbon Black solution (Spin-Coated thin-film)

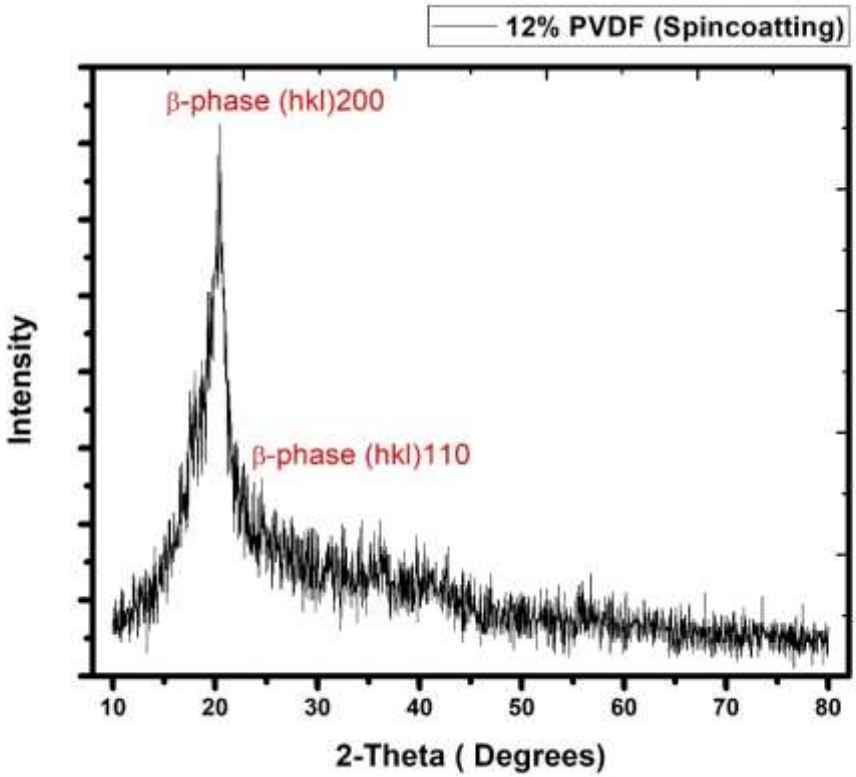

Figure 4.21: XRD pattern of the 12% PVDF solution (Spin-Coated thin-film)

4.1.4. UV-VIS spectrum of Thin-films and Nanofibers:

The graph below shows the transmittance of the UV-Visible spectrum of spin-coated electrospun samples in Figure 4.22 and 4.23 respectively. It is seen in below graphs that as we increased the concentration of polymer in solution the absorbance of light also increased, we get the peaks for all samples in the range of UV-Vis from 200 to 1000. Overall transmittance was 70 to 85%. Same results were reported in the literature (Punetha, et al., 2020) (Sabira, et al., 2017) and (Menazea, et al., 2020). The reason behind the direct relation of absorbance of light was the thickness of film increased with increase in concentration at the same parameters of spin-coating

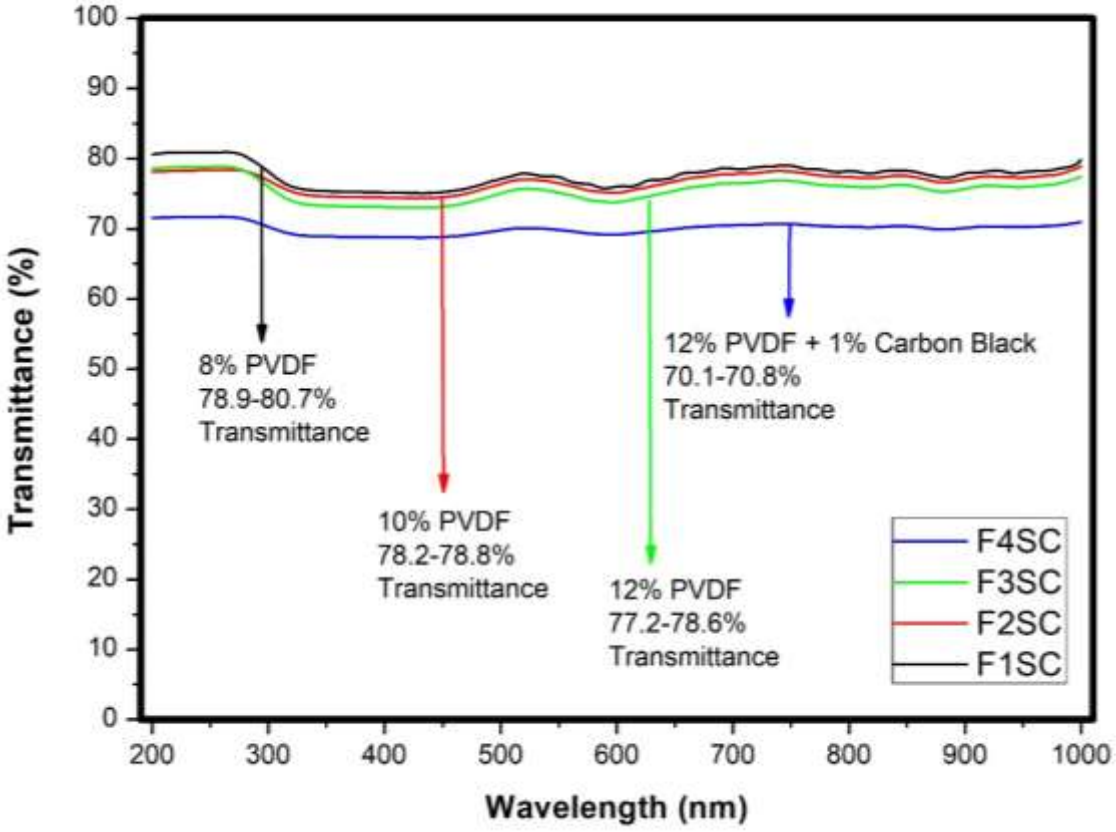

Figure 4.22: UV-Visible spectrum of the Spin-Coated thin-film PVDF

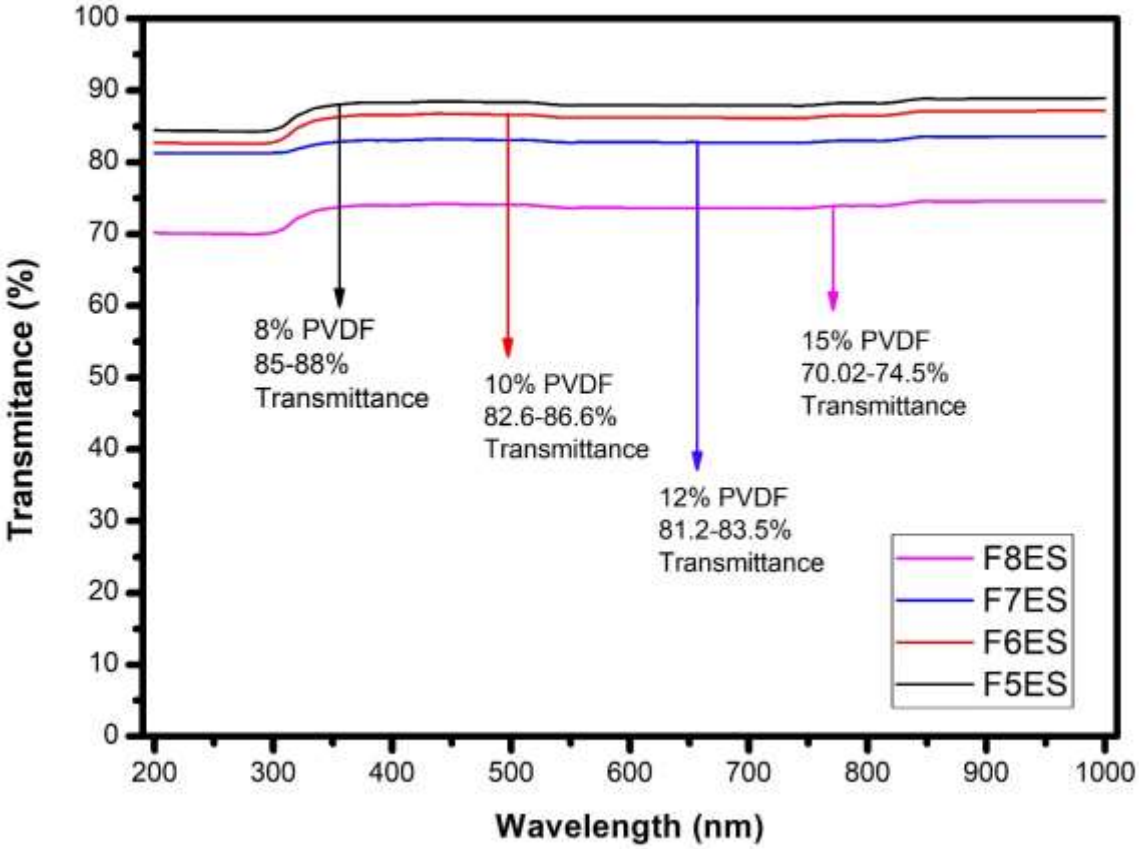

Figure 4.23: UV-Visible spectrum of the Electrospun Nanofibers PVDF

4.1.5. Hall-Effect of Nanofibers and Thin films:

The hall-effect of thin-films and nanofibers shows the results of resistance conductivity and mobility of samples.

4.1.5.1. Resistance:

With the help of hall-effect, it is mentioned that the resistance of the first three samples was very high.

The highest value of resistance is 9995.6 Ω.cm. There is the reason which we get from the information of FTIR spectra that the alpha phase is dominating in these samples. While sample F_4^{SC} that contain PVDF, as well as 1% of Carbon black, have low resistance as carbon black is the source of electrons because it has four extra electrons in his outermost shell. Sample F_5^{ES} also shows the slightly higher value of resistance as it also has the value of β-phase is 10.46% which is less than other electrospun fibres. Last three samples show lower values of resistance because of the enrichment of the β-phase.

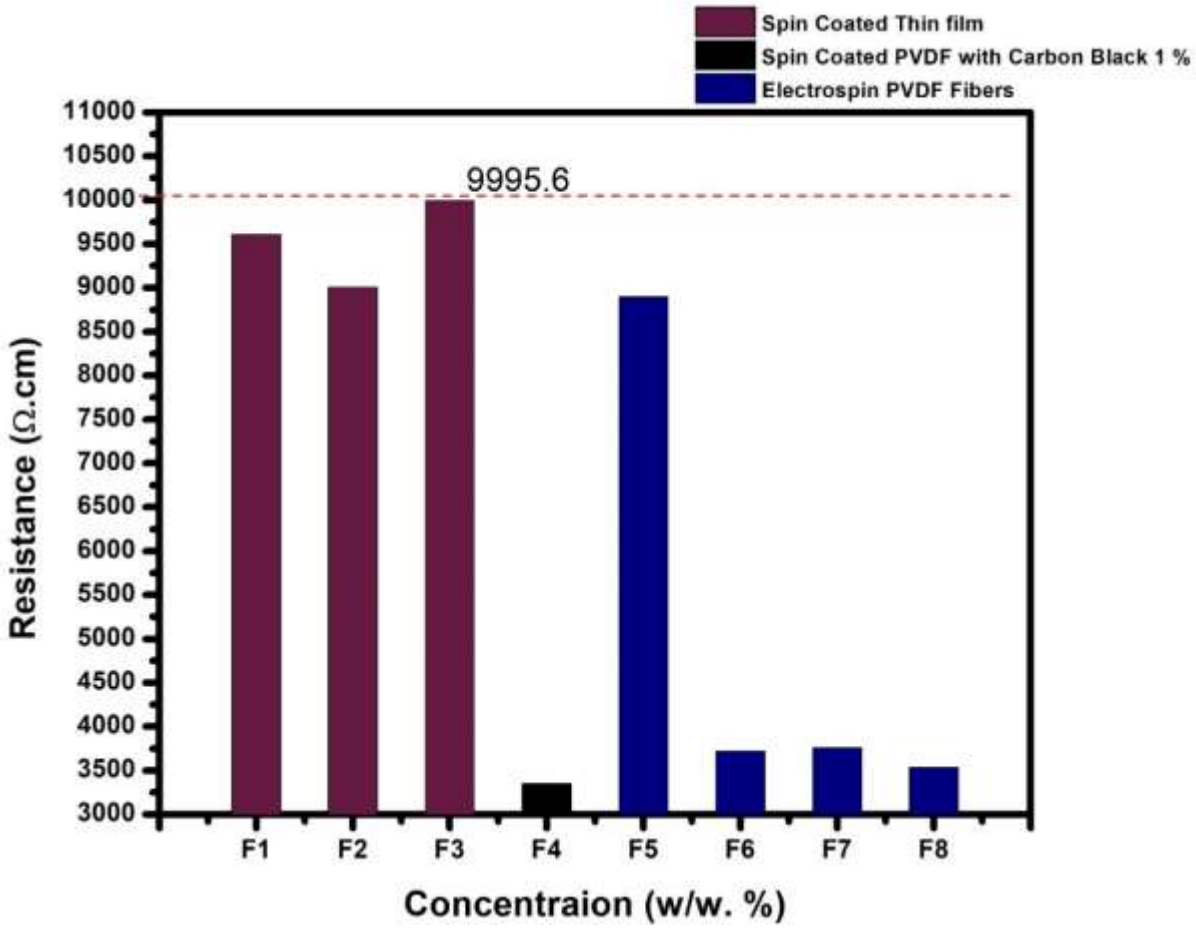

Figure 4.24 Hall-effect resistance of nano-fibres and thin-films

4.1.5.2. Conductivity:

The graph below shows the value of conductivity of samples which is higher in the sample F_4^{SC} i.e. PVDF with carbon black where carbon act as the source of a higher value of mobile electron. The value of F_4^{SC} sample is 4.7 x 10^{-4}. Here is the value of sample F_5^{ES} is at least one 0.9 x 10^{-4}.

We can see easily that as we increase the concentration of polymer in the solution the conductivity of thin-films decreases because in spin-coating method polymer remains in his alpha phase because of no change in the arrangement of atoms which is not an electro-active phase. The only value of carbon-doped thin-film is high indicated that addition of carbon promotes the conductivity of PVDF. The conductivity of nano-fibres increases with increase in the concentration of polymer because of electrospun change the polymer atomic arrangement from alpha to the beta phase which is electroactive.

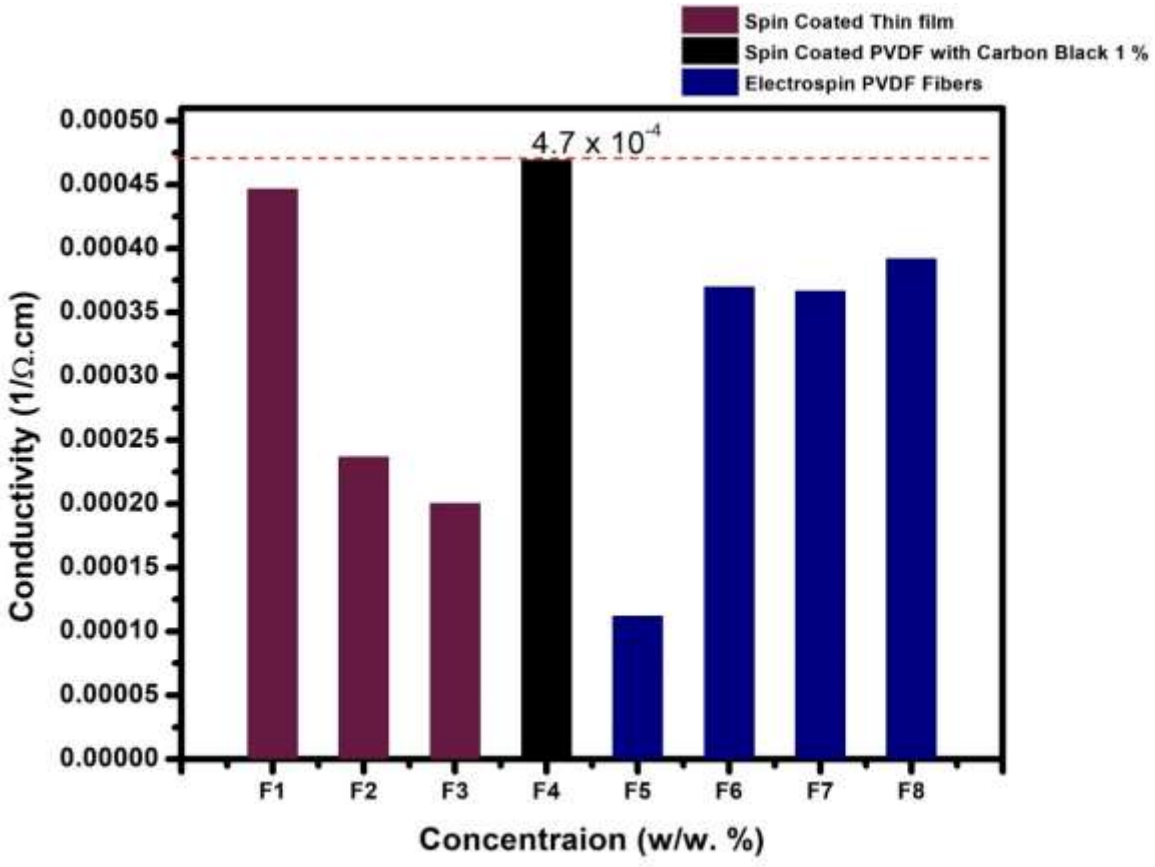

Figure 4.25: Hall-effect conductivity of nano-fibres and thin-films

4.1.5.3. Mobility:

The higher value of mobility of sample F4 was high i.e. 0.243 cm^2. Vs and the lower value is 0.023 cm^2.Vs.

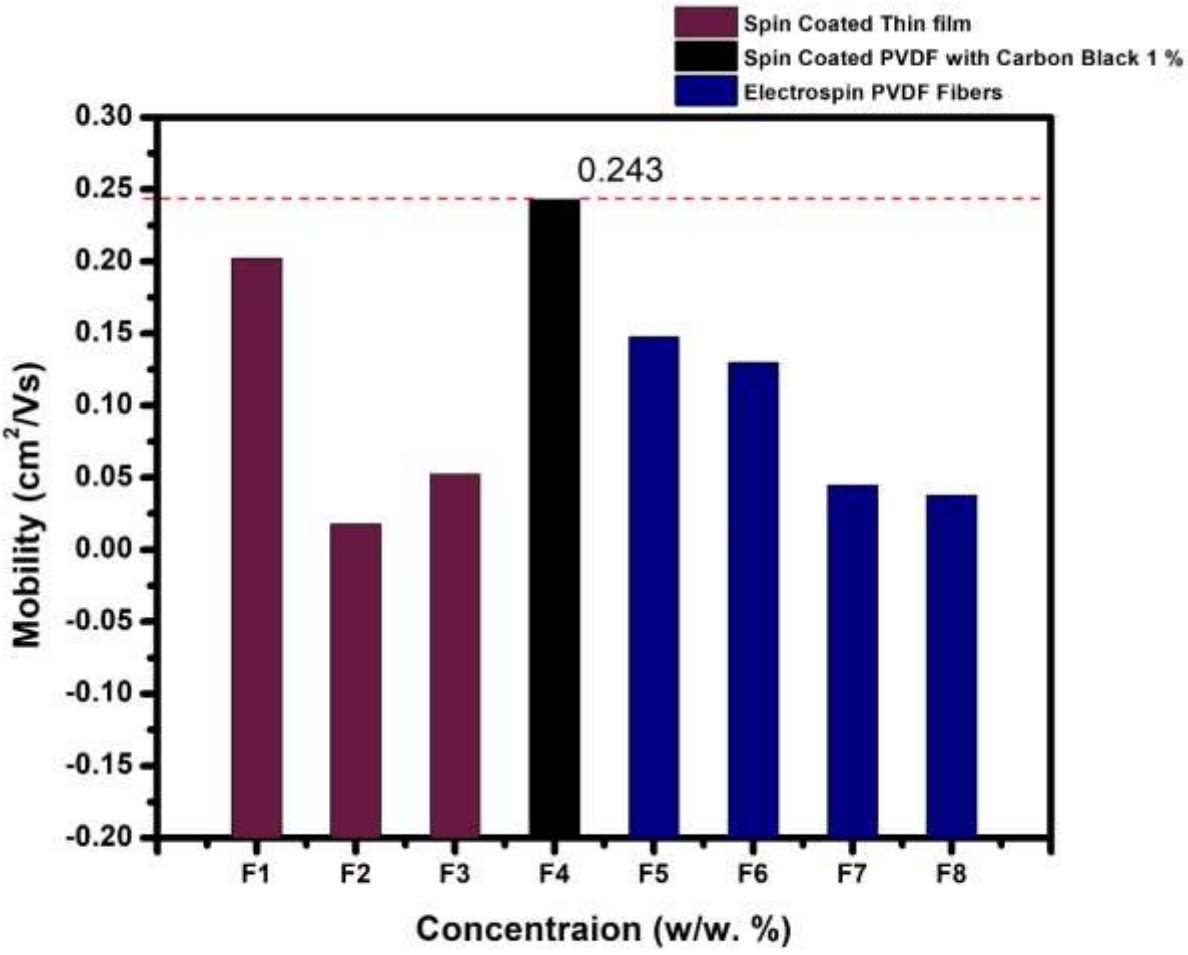

Figure 4.26: Hall-effect Mobility of nano-fibers and thin-films

4.1.6. The figure of Merits:

According to the following above characterization, we developed a figure of merits based on these parameters we can best identify which one is the best suitable option among all.

Table 4.3: Figure of Merits for evaluation of Effects of thin-film & nanofibers for solar cells

Sr.No.	***Sample Name***	***FTIR (β) %***	***Resitance Ω.cm***	***Conductivity 1/ Ω.cm***	***Mobility $Cm^2.Vs$***	***Remarks***
1	F_1^{SC}	1.27	9608.33	4.47×10^{-4}	0.20234	High Conductivity and mobility but low β-phase
2	F_2^{SC}	1.18	9005.67	2.37×10^{-4}	0.01761	High Resistance low mobility and β-phase
3	F_3^{SC}	2.47	9995.67	2.00×10^{-4}	0.05243	High Resistance low conductivity and mobility and low β-phase
4	F_4^{SC}	7.68	3350.33	4.69×10^{-4}	0.24296	Low Resistance highest in conductivity but low β-phase
5	F_5^{ES}	10.46	8897	1.12×10^{-4}	0.14776	High β-phase but also high in resistance
6	F_6^{ES}	16.12	3723.33	3.69×10^{-4}	0.1297	High β-phase low in resistance but High in Conductivity
7	F_7^{ES*}	17.42	3756	3.67×10^{-4}	0.04496	Highest in β-phase low in resistance than F1. Structure of fibres starts from very low

						diameter which promotes the flow of electron.
8	F_8^{ES}	12.42	3536.33	3.92×10^{-4}	0.03774	Low in the proportion of β-phase concentration also lowest in the mobility of charge

This FOM shows based on all of these parameters. We recommended that the optimum sample for better energy harvesting is:

- ✓ F_7^{ES} i.e. (12% PVDF) electrospun nano fibers

Same results were obtain by (Cai et al., 2017). So we can say that this is the best suitable option for interlayer in the solar cell as pyroelectric material to enhance the energy harvesting efficiency of cells. Even we can use this concentration to get more β-content by dopping with different transition elements and high organic crystalline polymers or co-polymers.

Chapter 5

CONCLUSION AND RECOMMENDATIONS

This study provides clear guidelines for using FTIR to solve long-term problems in the phase characterization of PVDF, and also provides a simple method for the single β and γ phases in multiphase PVDF polymers based on FTIR spectroscopy quantify.

Hall-effect shows mobility and conductivity of carbon black added into 12% PVDF dissolved into DMF/Acetone solution was high. But FTIR & XRD results indicate the crystalline phase in Carbon doped PVDF is less than electrospun nanofibers. Because the electrospinning process uses the electric field between two opposite charged electrodes to produce the nanofibers web which is in favour of the rearrangement of atoms in the polymer and produce β-phase of PVDF.

This phase of PVDF is more electroactive and pyroelectric. It shows more thermal energy harvesting wasted during the heat loss of the photoelectric effect. It also improves the efficiency of the solar cell. FTIR characterization shows β-content was high i.e. 17.42% in electrospun nanofibers of 12% PVDF. The spectroscopy also has shown that it has no significant absorbance in UV-Vis range. That means it will not cause any hurdle in the direct sunlight on the absorber layer. SEM results have shown the formation of the fibre of PVDF was not good at the concentration of 8% wt./wt. The fibres formation started at 10% wt./wt. of PVDF. The best fiber formation of PVDF was at the concentration of 12% wt./wt. But at 15% the thickness was very high and can cause resistance in the flow of direct current. So overall at the figure of merit we concluded that 12% PVDF of nanofibers and 12% of carbon-doped spin-coated was a suitable option with optimal output of selected parameters.

The β-content of PVDF can be increased by using different copolymers of PVDF like TrFE-PVDF, PMMA-PVDF, PVA-PVDF. Further, inorganic oxidizing and reducing agents from transition metals like Ti, Sb, V, and complexes of transition ions can be used. The group III-A and V-A like Al, Gr, As can also increase the β-phase formation in PVDF. The addition of reduce graphene oxide (RGO) to PVDF results in the enhancement of the β-phase of PVDF. Therefore, by increasing the β-content more low heat energy (lost during the energy transformation) can be harnessed.

References:

1. Abdin, Z., Alim, M. A., Saidur, R., Islam, M. R., Rashmi, W., Mekhilef, S., & Wadi, A. (2013). Solar energy harvesting with the application of nanotechnology. *Renewable and Sustainable Energy Reviews*, *26*, 837–852. https://doi.org/10.1016/j.rser.2013.06.023
2. Barber, P., Balasubramanian, S., Anguchamy, Y., Gong, S., Wibowo, A., Gao, H., … Loye, H. C. Zur. (2009). *Polymer composite and nanocomposite dielectric materials for pulse power energy storage*. *Materials* (Vol. 2). https://doi.org/10.3390/ma2041697
3. Beachley, V., & Wen, X. (2009). Effect of electrospinning parameters on the nanofiber diameter and length. *Materials Science and Engineering C*, *29*(3), 663–668. https://doi.org/10.1016/j.msec.2008.10.037
4. Bhavanasi, V., Kusuma, D. Y., & Lee, P. S. (2014). Polarization orientation, piezoelectricity, and energy harvesting performance of ferroelectric PVDF-TrFE nanotubes synthesized by nanoconfinement. *Advanced Energy Materials*, *4*(16), 1–8. https://doi.org/10.1002/aenm.201400723
5. Bölük, G., & Mert, M. (2014). Fossil & renewable energy consumption, GHGs (greenhouse gases) and economic growth: Evidence from a panel of EU (European Union) countries. *Energy*, *74*(C), 439–446. https://doi.org/10.1016/j.energy.2014.07.008
6. Cai, X., Lei, T., Sun, D., & Lin, L. (2017). A critical analysis of the α, β and γ phases in poly(vinylidene fluoride) using FTIR. *RSC Advances*, *7*(25), 15382–15389. https://doi.org/10.1039/c7ra01267e
7. Choubey, P. C., Oudhia, A., & Dewangan, R. (2009). Recent research in science and technology : an international refereed journal for all aspects of science research. *Recent Research in Science and Technology*, *4*(8), 99–101. Retrieved from https://scienceflora.org/journals/index.php/rrst/article/view/942
8. Choudhary, K., Bercx, M., Jiang, J., Pachter, R., Lamoen, D., & Tavazza, F. (2019). Accelerated Discovery of Efficient Solar Cell Materials Using Quantum and Machine-Learning Methods. *Chemistry of Materials*, *31*(15), 5900–5908. https://doi.org/10.1021/acs.chemmater.9b02166
9. Choudhary, P., & Srivastava, R. K. (2019). Sustainability perspectives- a review for solar photovoltaic trends and growth opportunities. *Journal of Cleaner Production*, *227*, 589–612. https://doi.org/10.1016/j.jclepro.2019.04.107
10. Conibeer, G. (2014). Third-Generation Solar Cells. *Solar Cell Materials:*

Developing Technologies, *9780470065*(6), 283–314. https://doi.org/10.1002/9781118695784.ch9

11. Conte, A. A., Shirvani, K., Hones, H., Wildgoose, A., Ye, X., Najjar, R., … Beachley, V. Z. (2019). Effects of post-draw processing on the structure and functional properties of electrospun PVDF-HFP nanofibers. *Polymer*, *171*(December 2018), 192–200. https://doi.org/10.1016/j.polymer.2019.03.017
12. Costa, L. M. M., Bretas, R. E. S., & Gregorio, R. (2010). Effect of Solution Concentration on the Electrospray/Electrospinning Transition and on the Crystalline Phase of PVDF. *Materials Sciences and Applications*, *01*(04), 247–252. https://doi.org/10.4236/msa.2010.14036
13. Dioxide, T., & Soga, T. (2006). Learn more about Solar Cell Fundamentals of Solar Cell Solar devices Nanophotonics : devices for manipulat- ing light at the nanoscale.
14. Fonash, S. J. (2010). *Cell Solar Physics Device physics*. Retrieved from http://libgen.me/view.php?id=290107
15. GFSE, G. F. on S. E. (2016). Key Points of the Paris Agreement, (March), 1–4. Retrieved from http://www.climateactiontracker.org/indcs/
16. Haider, A., Haider, S., & Kang, I. K. (2018). A comprehensive review summarizing the effect of electrospinning parameters and potential applications of nanofibers in biomedical and biotechnology. *Arabian Journal of Chemistry*, *11*(8), 1165–1188. https://doi.org/10.1016/j.arabjc.2015.11.015
17. IRENA. (2019). *Future of Solar Photovoltaic: Deployment, investment, technology, grid integration and socio-economic aspects*.
18. Jachalke, S., Mehner, E., Stöcker, H., Hanzig, J., Sonntag, M., Weigel, T., … Meyer, D. C. (2017). How to measure the pyroelectric coefficient? *Applied Physics Reviews*, *4*(2). https://doi.org/10.1063/1.4983118
19. Kang, S. B., Jeong, M. H., Choi, I. Y., Sohn, S. D., Kim, S. H., Shin, H. J., … Choi, K. J. (2017). Self-assembled, highly crystalline porous ferroelectric poly(vinylidene fluoride-co-trifluoroethylene) interlayer for Si/organic hybrid solar cells. *Nano Energy*, *41*(July), 243–250. https://doi.org/10.1016/j.nanoen.2017.09.033
20. Kang, S. J., Park, Y. J., Sung, J., Jo, P. S., Park, C., Kim, K. J., & Cho, B. O. (2008). Spin cast ferroelectric beta poly(vinylidene fluoride) thin films via rapid thermal annealing. *Applied Physics Letters*, *92*(1), 2006–2009. https://doi.org/10.1063/1.2830701

21. Khursheed, M. U. N., Nadeem Khan, M. F., Ali, G., & Khan, A. K. (2019). A review of estimating solar photovoltaic cell parameters. *2019 2nd International Conference on Computing, Mathematics and Engineering Technologies, ICoMET 2019*. https://doi.org/10.1109/ICOMET.2019.8673500
22. Krebs, F. C. (2009). Fabrication and processing of polymer solar cells: A review of printing and coating techniques. *Solar Energy Materials and Solar Cells*, *93*(4), 394–412. https://doi.org/10.1016/j.solmat.2008.10.004
23. Landsberg, P. T., & Markvart, T. (2017). *Ideal efficiencies*. *McEvoy's Handbook of Photovoltaics: Fundamentals and Applications*. Elsevier Ltd. https://doi.org/10.1016/B978-0-12-809921-6.00003-3
24. Lare, M.-C. van. (2014). *Light Trapping in Solar Cells Using Dielectric And Metallic Nanostructures*.
25. Li, Y., & Zhang, B. (2020). Defects reparation and surface hydrophilic modification of zeolite beta membranes with spherical polyelectrolyte complex nanoparticles via vacuum-wiping deposition technique. *Journal of Membrane Science*, *602*(February), 117977. https://doi.org/https://doi.org/10.1016/j.memsci.2020.117977
26. Mahesh, D., & Rajesh, J. (2012). TiO 2 Microstructure, Fabrication of thin Film Solar Cells and Introduction to Dye Sensitized Solar Cells. *Research Journal of Recent Sciences Res.J.Recent.Sci*, *2*(2012), 25–29.
27. Matabola, K. P., & Moutloali, R. M. (2013). The influence of electrospinning parameters on the morphology and diameter of poly(vinyledene fluoride) nanofibers- Effect of sodium chloride. *Journal of Materials Science*, *48*(16), 5475–5482. https://doi.org/10.1007/s10853-013-7341-6
28. Menazea, A. A., Ismail, A. M., & Elashamwi, I. S. (2020). The role of Li4Ti5O12 nanoparticles on enhancement the performance of PVDF/PVK blend for lithium-ion batteries. *Journal of Materials Research and Technology*, (x x). https://doi.org/10.1016/j.jmrt.2020.03.093
29. Mozumder, M. S., Mourad, A. H. I., Pervez, H., & Surkatti, R. (2019). Recent developments in multifunctional coatings for solar panel applications: A review. *Solar Energy Materials and Solar Cells*, *189*(October 2018), 75–102. https://doi.org/10.1016/j.solmat.2018.09.015
30. Ni, C. (2013). Scanning Electron Microscopy (SEM). In Q. J. Wang & Y.-W. Chung (Eds.), *Encyclopedia of Tribology* (pp. 2977–2982). Boston, MA: Springer US. https://doi.org/10.1007/978-0-387-92897-5_1217

31. Petrus, M. L. (2009). Polymer solar cells Polymer solar cells. *Master Thesis*, *56*(3), 45–108.
32. Prashant, A. (2018). Literature Review on Photovoltaic Panels. *International Journal of Emerging Research in Management &Technology*, *9359*(7), 2278–9359. Retrieved from www.ermt.net
33. Punetha, D., Kar, M., & Pandey, S. K. (2020). A new type low-cost, flexible and wearable tertiary nanocomposite sensor for room temperature hydrogen gas sensing. *Scientific Reports*, *10*(1), 1–11. https://doi.org/10.1038/s41598-020-58965-w
34. Ranabhat, K., Patrikeev, L., Revina, A. A. evna, Andrianov, K., Lapshinsky, V., & Sofronova, E. (2016). An introduction to solar cell technology. *Journal of Applied Engineering Science*, *14*(4), 481–491. https://doi.org/10.5937/jaes14-10879
35. Rex Rosario, S., Kulandaisamy, I., Deva Arun Kumar, K., Arulanantham, A. M. S., Valanarasu, S., Youssef, M. A., & Awwad, N. S. (2019). Deposition of p-type Al doped PbS thin films for heterostructure solar cell device using feasible nebulizer spray pyrolysis technique. *Physica B: Condensed Matter*, *575*(July), 411704. https://doi.org/10.1016/j.physb.2019.411704
36. Ruan, L., Yao, X., Chang, Y., Zhou, L., Qin, G., & Zhang, X. (2018). Properties and applications of the β phase poly(vinylidene fluoride). *Polymers*, *10*(3), 1–27. https://doi.org/10.3390/polym10030228
37. Sabira, K., Saheeda, P., Divyasree, M. C., & Jayalekshmi, S. (2017). Impressive nonlinear optical response exhibited by Poly(vinylidene fluoride) (PVDF)/reduced graphene oxide (RGO) nanocomposite films. *Optics and Laser Technology*, *97*, 77–83. https://doi.org/10.1016/j.optlastec.2017.06.008
38. Saga, T. (2010). Advances in crystalline silicon solar cell technology for industrial mass production. *NPG Asia Materials*, *2*(3), 96–102. https://doi.org/10.1038/asiamat.2010.82
39. Schmidt, J., Marques, M. R. G., Botti, S., & Marques, M. A. L. (2019). Recent advances and applications of machine learning in solid-state materials science. *Npj Computational Materials*, *5*(1). https://doi.org/10.1038/s41524-019-0221-0
40. Sengupta, D., Michael, A., Kwok, C. Y., Miao, J., & Kottapalli, A. G. P. (2018). Optimized Polyvinylidene Fluoride Nanofiber Webs for Flexible Energy Harvesters. *Proceedings*, *2*(13), 857. https://doi.org/10.3390/proceedings2130857
41. Sharma, M., Srinivas, V., Madras, G., & Bose, S. (2016). Outstanding dielectric

constant and piezoelectric coefficient in electrospun nanofiber mats of PVDF containing silver decorated multiwall carbon nanotubes: Assessing through piezoresponse force microscopy. *RSC Advances*, *6*(8), 6251–6258. https://doi.org/10.1039/c5ra25671b

42. Siddiqui, F. I. (2019). Energy challenges & opportunities Iraqi Oil Minister Value addition, (7).
43. Soga, T. (n.d.). Tetsuo Soga Department of Environmental Technology and Urban Planning Nagoya Institute of Technology Gokiso-cho, Showa-ku, Nagoya 466-8555, Japan, 2. https://doi.org/10.1016/B978-0-444-52844-5.50001-9
44. Summary, R. (2016). Research opportunities to advance solar energy utilization. *Science*, *351*(6271), add1920-1–9. https://doi.org/10.1126/science.aad1920.22
45. Terakawa, A. (2013). Review of thin-film silicon deposition techniques for high-efficiency solar cells developed at Panasonic/Sanyo. *Solar Energy Materials and Solar Cells*, *119*, 204–208. https://doi.org/10.1016/j.solmat.2013.06.044
46. Wang, Y. R., Zheng, J. M., Ren, G. Y., Zhang, P. H., & Xu, C. (2011). A flexible piezoelectric force sensor based on PVDF fabrics. *Smart Materials and Structures*, *20*(4). https://doi.org/10.1088/0964-1726/20/4/045009
47. Yan, J., Liu, M., Jeong, Y. G., Kang, W., Li, L., Zhao, Y., … Yang, G. (2019). Performance enhancements in poly(vinylidene fluoride)-based piezoelectric nanogenerators for efficient energy harvesting. *Nano Energy*, *56*(October 2018), 662–692. https://doi.org/10.1016/j.nanoen.2018.12.010
48. Zhang, W., Wang, J., Gao, P., Tan, S., Zhu, W., & Zhang, Z. (2017a). Synthesis of poly(vinylidene fluoride-trifluoroethylene): Via a controlled silyl radical reduction of poly(vinylidene fluoride-chlorotrifluoroethylene). *Journal of Materials Chemistry C*, *5*(26), 6433–6441. https://doi.org/10.1039/c7tc01051f
49. Zhang, W., Wang, J., Gao, P., Tan, S., Zhu, W., & Zhang, Z. (2017b). Synthesis of poly(vinylidene fluoride-trifluoroethylene): Via a controlled silyl radical reduction of poly(vinylidene fluoride-chlorotrifluoroethylene). *Journal of Materials Chemistry C*, *5*(26), 6433–6441. https://doi.org/10.1039/c7tc01051f